

# Queues with Rechargeable Servers

Eliezer Fuentes-Quezada

School of Operations Research and Information Engineering  
Cornell University  
eif8@cornell.edu

Jamol Pender <sup>\*</sup>

School of Operations Research and Information Engineering  
Cornell University  
jjp274@cornell.edu

February 12, 2026

## Abstract

Drone delivery systems violate a core assumption in classical queueing models: server capacity is not fixed. Drones (servers) periodically must recharge, creating random fluctuations in service availability. We introduce an Erlang–S\* queue that incorporates charging dynamics (probability of charging after service completion  $p$  and charging return rate  $\gamma$ ) together with abandonment. We derive fluid and diffusion limits, yielding closed-form steady-state means, variances, and covariances for the joint queue–server process  $(Q, S)$ . The diffusion limits allow us to derive new staffing rules for the probability of delay and the probability of abandonment targets. A key insight is that server stochasticity induces systematic capacity loss relative to fixed-server systems, leading to a regime–dependent staffing adjustment: additive shifts in underloaded regimes and multiplicative scaling in overloaded regimes. Our simulation experiments confirm both the accuracy of the limit theorems and the performance of the staffing schedule’s ability to achieve their targets.

---

<sup>\*</sup>Corresponding Author

# 1 Introduction

Drone delivery, an emerging logistics innovation, relies on unmanned aerial vehicles (UAVs) to transport goods directly to consumers, bypassing traditional road networks and leveraging the sky, Grippa et al. [19], Cokyasar et al. [12], Pinto et al. [39], Huang et al. [20], Shavarani et al. [42], Seakhoa-King et al. [41], Khamidehi et al. [21], Munishkin et al. [29], Ghosh et al. [17]. From a queueing theory perspective, drone delivery introduces a new class of service mechanisms. Unlike traditional delivery methods such as vans and trucks that follow fixed routes and perform batch deliveries, drones may serve requests individually and adaptively, resembling a multi-server queueing system with spatially distributed arrivals. This shift requires re-thinking classical queueing models to include factors such as drone battery life (leading to server vacations), weather dependent service rates, and real-time demand clustering. Understanding the implications of these factors is crucial for designing efficient drone delivery systems.

Drone delivery is particularly important for urgent deliveries such as medical supplies to remote or hard to traverse places. For example, Zipline in Rwanda, operates a drone delivery service that helps deliver vital medical supplies like blood and vaccines to remote and hard to reach medical facilities. The drone delivery improves access to healthcare and ensuring critical supplies reach patients much faster than traditional delivery methods, see for example [10, 11, 4, 25, 9, 24]. Moreover, it has reduced maternal mortality by ensuring timely access to healthcare supplies, Zailani et al. [50].

In addition, drone delivery offers environmental benefits by reducing carbon emissions compared to traditional delivery vehicles. Drones are typically electric-powered, which can lead to lower greenhouse gas emissions, especially when charged using renewable energy sources, Goodchild and Toy [18], Figliozzi [16], Brown and Bushuev [8]. This makes drone delivery an attractive option for companies looking to reduce their environmental footprint while also improving delivery speed and efficiency. However, drone delivery systems face unique challenges that impact their queueing dynamics. One of the most significant challenges is the limited battery life of drones, which necessitates periodic recharging. This introduces a stochastic element to server availability, as drones (servers) may leave the system to recharge after completing deliveries, leading to fluctuations in service capacity. Additionally, factors such as weather conditions, air traffic regulations, and payload limitations further complicate the service process. These challenges require new

queueing models that can accurately capture the dynamics of drone delivery systems and inform effective staffing and scheduling strategies.

Drone Model	Charging Time	Flight Time	Max Payload
DJI Mavic Air 2	1 hr 40 min	34 min	0.2 kg
DJI Matrice 300 RTK	1.5 hrs (per battery)	55 min	2.7 kg
Autel EVO II Pro	1.5 hrs	40 min	0.9 kg
Parrot Anafi USA	2 hrs	32 min	0.5 kg
Skydio X10	1.5 hrs	40 min	0.4 kg

Table 1: Drone Models Specifications

Table 1 summarizes the operational characteristics of several commercial drone models, highlighting their charging times, flight durations, and payload capacities, DJI [14], Autel Robotics [2], Parrot [32], Skydio [43]. These specifications directly influence the performance of a drone-based service system modeled as a queue, where drones act as servers that periodically leave to recharge. For instance, the DJI Matrice 300 RTK, with a flight time of 55 minutes and a payload of 2.7 kg, represents a high-capacity but energy-demanding server, while the DJI Mavic Air 2 and Skydio X10, with shorter flight times and lighter payloads, correspond to lower-capacity servers that must recharge more frequently. These heterogeneities translate into variability in effective service rates and server availability, key determinants of system congestion and customer waiting times.

In the context of the queueing model analyzed in this paper, the data in Table 1 illustrate how drone design and energy constraints shape the stochastic dynamics of the service process. Longer charging durations increase the fraction of time drones are unavailable, effectively reducing the system’s active service capacity. Conversely, models with shorter recharging cycles or longer flight durations contribute to smoother operations and lower abandonment probabilities. By capturing such trade-offs, Table 1 provides a realistic basis for parameterizing the model’s service and recharge rates, enabling the analysis of fluid and diffusion limits that inform energy-aware staffing.

On the other hand, with respect to the customer experience, capturing and managing wait time for deliveries is crucial. Customers expect timely deliveries, and any delays can lead to dissatisfaction and loss of business, see for example Massey and Pender [27], Van Leeuwaarden and Knessl [48], Pender [33, 34], Knessl and van Leeuwaarden [22], Pender [35], Massey and

Pender [28], Legros and Jouini [23]. Therefore, understanding and optimizing the queueing dynamics in drone delivery systems is essential for maintaining high service levels and customer satisfaction. Unfortunately, there are very few papers that study drone delivery with a queueing emphasis. In particular, we find it important to include abandonment and charging times of drones (server vacations). Research by Dimou et al. [13], Dudin et al. [15] explores queueing models with abandonment and server vacations, however, these papers either consider discrete time queueing models or single server queueing models. The paper by Altman and Yechiali [1] does consider multiple servers, however, the model assumes that all idle servers go for vacations, which is not practical for this drone delivery setting.

Finally, Azriel et al. [3] studies queueing systems with stochastic server availability through an exponential vacation model motivated by call-center applications. In their framework, servers enter vacations after service completion with a fixed probability, a modeling assumption that is shared with the present paper. However, server availability in their model is restored through multiple mechanisms: servers may return from vacation spontaneously at an exponential rate, or become available immediately with a certain probability when customers are waiting in the queue. In contrast, in our model servers return from charging exclusively at an exponential rate, independent of the queue length. This modeling choice, while simpler, leads to fundamentally different system dynamics: server availability is coupled to service completions but decoupled from instantaneous queue congestion, reflecting the operational realities of drone recharging. As a result, the induced queue-server dependence, as well as the resulting fluid and diffusion limits, differ substantially from those that arise in vacation-based models with queue-dependent server return mechanisms.

Thus, in this paper, we introduce a new queueing framework that captures a fundamental feature of drone delivery systems: stochastic server availability driven by post-service charging requirements. We model drones as servers that probabilistically enter a charging state after completing service and return to availability at an exponential rate, while customers may abandon if their waiting time exceeds their patience. Within this framework, we characterize system behavior using fluid and diffusion limit theorems, deriving explicit expressions for the steady-state means, variances, and covariances of the joint queue length and server availability process. These results enable tractable staffing policies that achieve prescribed targets for delay and abandonment probabilities.

While motivated by drone delivery, the modeling framework and analytical insights developed in this paper extend naturally to a broad class of service systems with intermittently unavailable servers. In healthcare settings, for example, medical staff, diagnostic equipment, or operating rooms often require recovery, cleaning, or setup periods following service completion, during which they are temporarily unavailable. Similarly, in robotic and automated service systems, robots must periodically recharge or undergo maintenance after completing tasks, leading to endogenous fluctuations in service capacity. Related dynamics arise in shared mobility and micromobility systems, such as e-bike or scooter fleets (see for example Sun et al. [44], Tao and Pender [46], Pender et al. [37], Tao and Pender [47], Xie et al. [49], Tao [45], Pla et al. [40], Liu et al. [26]), where vehicles become unavailable while charging or undergoing battery swaps.

More broadly, the Erlang–S\* framework captures service environments in which server availability is coupled to workload through post-service recovery, rather than determined solely by idleness or external scheduling. By explicitly accounting for this coupling and the resulting queue/server dependence, the proposed model provides a foundation for energy-aware and reliability-driven staffing decisions in modern service systems. The analytical tractability of the fluid and diffusion approximations makes the framework particularly suitable for large-scale systems where capacity planning must balance congestion, abandonment, and resource recovery constraints.

## 1.1 Contributions of the Paper

In this section, we outline the major contributions of the paper.

1. A stochastic model (Erlang–S\*) where servers take i.i.d. stochastic “vacations” to charge.
2. Fluid limits with steady-state closed forms that highlight the systematic capacity drain from charging.
3. Diffusion (OU) limits providing regime-specific formulas for  $\text{Var}(Q)$ ,  $\text{Var}(S)$ ,  $\text{Cov}[Q, S]$ .
4. Staffing rules for meeting delay and abandonment targets that explicitly incorporate covariance.
5. We validate our results with stochastic simulation.

## 1.2 Organization of the Paper

In this section, we provide an outline of how this paper is organized. Section 2 defines the stochastic model, its dynamics and model primitives. Section 3 presents the fluid limit and analyzes the steady-state regimes of the fluid limit. Section 4 derives diffusion limits and derives new insights about the structure of the covariance. Section 5 develops staffing schedules (deterministic and bivariate-normal) to stabilize delay probabilities. Section 6 develops staffing schedules to stabilize abandonment probabilities. Finally, Section 7 reports numerical experiments and all non-trivial proof details are provided in the Appendix.

## 2 The Erlang–S\* Model

We consider a modified Erlang-A or Erlang-S queue with  $c$  servers, where each server may go to a charging state after completing service. This models scenarios such as drone delivery systems with battery constraints. Just as in the Erlang-A queue,  $\lambda$  is the arrival rate,  $\mu$  is the service rate,  $\theta$  is the abandonment rate,  $c$  is the total number of servers. Our extension has two additional parameters. The first  $p$  is the probability that the server goes to charge after completing their service. The second additional parameter is  $\gamma$ , which represents the rate at which the charging server completely charges and goes back to being available for service.

### 2.1 Stochastic Model Construction

Arrivals follow a Poisson process of rate  $\lambda$ . There are  $c$  identical servers (drones). Service times are exponential with rate  $\mu$ . Waiting customers abandon with rate  $\theta$  per customer. After each service completion, a server independently goes to charge with probability  $p$ ; charging duration is exponential with rate  $\gamma$ , after which the server returns active. Let  $Q(t)$  be total customers in system,  $S(t)$  active servers, and  $C(t) = c - S(t)$  charging servers; state space is  $\mathbb{Z}_{\geq 0} \times \{0, 1, \dots, c\}$ .

The model studied in this paper can be viewed as a simplified variant of the Erlang–S model introduced in Azriel et al. [3], in which server availability is governed by vacation dynamics inspired by call-center applications. In the Erlang–S framework, servers may enter or exit vacation states based on both

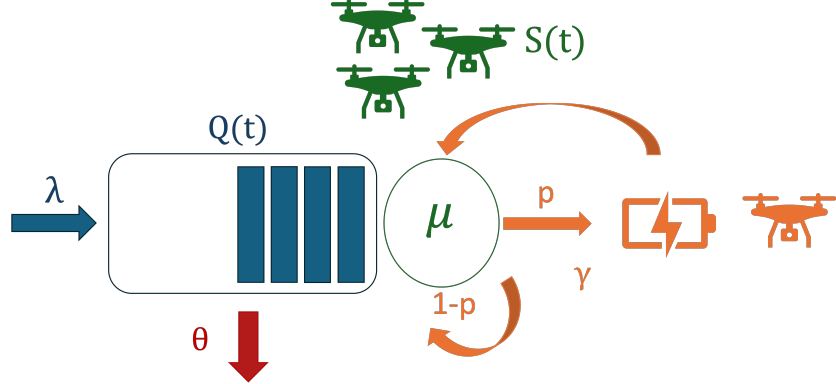


Figure 1: Schematic representation of the Erlang- $S^*$  model.

exogenous rates and the congestion level of the system, typically through mechanisms that depend on whether  $(Q(t) - S(t))^+ \neq 0$ .

In contrast, in our model the decision of a server to enter a charging state occurs probabilistically upon service completion and is independent of the instantaneous system state. Servers return from charging after an exponentially distributed time, also independently of queue congestion. This modeling choice removes explicit state-dependent vacation controls while preserving the essential feature of stochastic server availability induced by energy constraints. As a result, the model remains analytically tractable while capturing the dominant operational effects of drone recharging on system performance.

## 2.2 Stochastic Dynamics

Let  $\{N_A(t), N_B(t), N_C(t), N_{Ab}(t)\}_{t \geq 0}$  be independent unit-rate Poisson processes for arrivals, service completions, charge completions, and abandonments, respectively. Let  $\{\xi_i\}$  be i.i.d.  $\text{Bernoulli}(p)$  indicating whether the completing server goes to charge, with  $P(\xi_i = 1) = p$ ,  $P(\xi_i = 0) = 1 - p$ , indicating whether the server goes to charging after the  $i^{\text{th}}$  service comple-

tion. Then

$$Q(t) = Q(0) + N_A(\lambda t) - N_B \left( \mu \int_0^t \min\{Q(s), S(s)\} ds \right) - N_{Ab} \left( \theta \int_0^t (Q(s) - S(s))^+ ds \right), \quad (1)$$

$$S(t) = S(0) + N_C \left( \gamma \int_0^t (c - S(s)) ds \right) - \sum_{i \leq N_B \left( \mu \int_0^t \min\{Q(s), S(s)\} ds \right)} \xi_i. \quad (2)$$

We can interpret the dynamics as follows: service completions remove customers; a fraction  $p$  of completions send the server to charge; charging returns occur at rate  $\gamma$  per charging server; abandonments occur at rate  $\theta$  per waiting customer. The server process is autonomous but not independent of the queue due to service completions.

### 2.3 Explanation

- The term  $N_A(\lambda t)$  counts arrivals up to time  $t$ .
- Service completions occur at rate proportional to the number of busy servers,  $\mu \min(Q(t), S(t))$ , which drives the time change in  $N_B$ .
- Each service completion causes the server either to go to charging (with probability  $p$ ) or remain active. This is captured by the Bernoulli sequence  $\{\xi_i\}$ .
- Customers waiting in queue abandon at rate  $\theta$  per waiting customer, represented by  $N_{Ab}$  time-changed by the total waiting customer time.
- Charging servers return to active state at rate  $\gamma$  per charging server, represented by  $N_C$  time-changed by the total charging time.

It is important to note that, in this model, unlike the classical Erlang-A system with fixed capacity, stochastic server availability creates feedback between congestion and capacity, so that variability and covariance directly affect system performance. In the following two sections, we study these second-order effects in detail.

### 3 Fluid Approximation

We analyze the Erlang–S\* system under fluid scaling. Let  $\bar{Q}^n(t) = Q^n(t)/n$  and  $\bar{S}^n(t) = S^n(t)/n$  denote the scaled queue length and server processes. Their dynamics are described by the following equations.

$$\begin{aligned} Q^n(t) &= Q^n(0) + N_A(\lambda nt) - N_B \left( \mu \int_0^t \min(Q^n(s), S^n(s)) ds \right) \\ &\quad - N_{Ab} \left( \theta \int_0^t (Q^n(s) - S^n(s))^+ ds \right), \end{aligned} \quad (3)$$

$$S^n(t) = S^n(0) + N_C \left( \gamma \int_0^t (c - S^n(s)/n) ds \right) - \sum_{i=1}^{N_B(\mu \int_0^t \min(Q^n(s), S^n(s)) ds)} \xi_i. \quad (4)$$

With initial conditions  $\bar{Q}^n(0) \Rightarrow q(0)$ ,  $\bar{S}^n(0) \Rightarrow s(0)$ , we have the following fluid limit theorem.

**Theorem 3.1** (Fluid Limit for the Erlang–S Queue). *Consider the scaled stochastic processes*

$$\bar{Q}^n(t) = \frac{Q^n(t)}{n}, \quad \bar{S}^n(t) = \frac{S^n(t)}{n}.$$

*Then for every fixed  $T > 0$ ,*

$$\sup_{0 \leq t \leq T} \|(\bar{Q}^n(t), \bar{S}^n(t)) - (\bar{q}(t), \bar{s}(t))\| \xrightarrow{P} 0,$$

*where  $(\bar{q}, \bar{s})$  is the unique solution on  $[0, T]$  of*

$$\frac{dq(t)}{dt} = \lambda - \mu \min\{q(t), s(t)\} - \theta (q(t) - s(t))^+, \quad (5)$$

$$\frac{ds(t)}{dt} = \gamma (c - s(t)) - p\mu \min\{q(t), s(t)\}. \quad (6)$$

*Proof.* The proof can be found in Appendix A.1.  $\square$

Under standard functional LLNs for Poisson processes and random sums,  $(\bar{Q}^n, \bar{S}^n)$  converges to the unique solution  $(q, s)$  of (5) and (6), which we will analyze next.

### 3.1 Steady-State Regimes

In this section, we analyze the steady state limit of the fluid limit we obtained in the previous section.

$$\begin{aligned}\frac{dq(t)}{dt} &= \lambda - \mu(q(t) \wedge s(t)) - \theta(q(t) - s(t))^+ \\ \frac{ds(t)}{dt} &= \gamma(c - s(t)) - p\mu(q(t) \wedge s(t)).\end{aligned}\tag{7}$$

**Theorem 3.2.** *Let  $(q^*, s^*)$  be the steady state limits of Equations 7, if  $\frac{\lambda}{\mu} + \frac{\lambda p}{\gamma} \leq c$ , then*

$$q^* = \frac{\lambda}{\mu}\tag{8}$$

$$s^* = c - \frac{\lambda p}{\gamma}\tag{9}$$

and if  $\frac{\lambda}{\mu} + \frac{\lambda p}{\gamma} > c$ , then we have

$$q^* = \frac{\lambda - \frac{\gamma\mu c}{\gamma + p\mu}}{\theta} + \frac{\gamma c}{\gamma + p\mu}\tag{10}$$

$$s^* = \frac{\gamma c}{\gamma + p\mu}.\tag{11}$$

*Proof.* We will divide the proof into underloaded (UL) and overloaded (OL) cases. The first case considers the situation where there is no abandonment and the second case is where there is abandonment. In the case with no abandonment in steady state, we have  $q^* \leq s^*$ . Using this, we have in the differential equations set to zero that

$$0 = \lambda - \mu q^*\tag{12}$$

$$0 = \gamma(c - s^*) - p\mu q^*.\tag{13}$$

This proves the first case and since  $q^* \leq s^*$ , this is also the same condition in the statement of the result. The second case assumes that there is abandonment and therefore  $q^* \geq s^*$ . This implies

$$0 = \lambda - \mu s^* - \theta(q^* - s^*)\tag{14}$$

$$0 = \gamma(c - s^*) - p\mu s^*.\tag{15}$$

□

*Remark.* In the underloaded regime, the steady-state effect of stochastic charging manifests as an additive reduction in the effective number of available servers, given by  $\lambda p / \gamma$ . In contrast, in the overloaded regime, charging induces a multiplicative scaling of server availability by the factor  $\gamma / (\gamma + p\mu)$ , reflecting the long-run fraction of time that servers are available.

## 4 Diffusion Limits and the Covariance Structure

The Erlang–S\* model induces nontrivial dependence between the queue length and the number of available servers, so that second-order performance measures (variances and covariances) are intrinsic to the model rather than degenerate as in classical Erlang systems with fixed capacity. We therefore study the diffusion-scale fluctuations of the joint process around its fluid equilibrium.

Under the many-server scaling, define the fluid-scaled processes

$$\bar{Q}^n(t) = \frac{Q^n(t)}{n}, \quad \bar{S}^n(t) = \frac{S^n(t)}{n},$$

and let  $(q^*, s^*)$  denote the (globally attractive) equilibrium point of the corresponding fluid limit in the operating regime under consideration (underloaded or overloaded). Define the diffusion-scaled fluctuation process

$$\hat{X}^n(t) = \sqrt{n} \begin{pmatrix} \bar{Q}^n(t) \\ \bar{S}^n(t) \end{pmatrix} - \begin{pmatrix} q^* \\ s^* \end{pmatrix} \in \mathbb{R}^2.$$

The next theorem shows that  $\hat{X}^n$  converges to a two-dimensional Ornstein–Uhlenbeck process with drift determined by the Jacobian of the fluid drift on the active face and covariance determined by the primitive Poisson noises evaluated at  $(q^*, s^*)$ . The stationary covariance matrix of the limit is obtained by solving the Lyapunov equation  $JV + VJ^\top + \Sigma = 0$ .

**Theorem 4.1** (Diffusion limit for the Erlang–S\* queue). *Let*

$$\hat{X}^n(t) = \sqrt{n} \begin{pmatrix} \bar{Q}^n(t) \\ \bar{S}^n(t) \end{pmatrix} - \begin{pmatrix} q^* \\ s^* \end{pmatrix}, \quad t \in [0, T],$$

where  $(q^*, s^*)$  is the equilibrium point of the fluid limit. Then, as  $n \rightarrow \infty$ ,

$$\hat{X}^n \Rightarrow \hat{X} \quad \text{in } D([0, T], \mathbb{R}^2),$$

where  $\hat{X}$  is the unique strong solution of the linear SDE

$$d\hat{X}(t) = J \hat{X}(t) dt + \Sigma^{1/2} dW(t),$$

with  $J$  the Jacobian of the (piecewise) drift on the active face at  $(q^*, s^*)$  and  $\Sigma$  the diffusion matrix induced by the primitive Poisson noises evaluated at  $(q^*, s^*)$ .

*Proof.* The proof can be found in Appendix A.2.  $\square$

Following standard OU theory, the stationary second moments satisfy  $JV + VJ^\top + \Sigma = 0$ . We now have the computation of the stationary variances and covariance in each regime.

## 4.1 Underloaded Regime ( $q^* < s^*$ )

**Theorem 4.2.** *Consider the same setup as in the previous theorem. In the underloaded regime, the Jacobian and diffusion matrices are*

$$J = \begin{pmatrix} -\mu & 0 \\ -p\mu & -\gamma \end{pmatrix}, \quad \Sigma = \begin{pmatrix} \lambda + \mu q^* & -\mu q^* \\ -\mu q^* & p\mu q^* + \gamma(c - s^*) \end{pmatrix},$$

which yields the following stationary second moments:

$$\text{Var}(Q) \approx v_{qq}^* = \frac{\lambda}{\mu}, \quad \text{Var}(S) \approx v_{ss}^* = \frac{\lambda p}{\gamma}, \quad \text{Cov}[Q, S] = v_{qs}^* \approx 0.$$

*Proof.* The proof can be found in Appendix A.3.  $\square$

## 4.2 Overloaded Regime ( $q^* > s^*$ )

**Theorem 4.3.** *Consider the same setup as in the previous theorem. In the overloaded regime, the Jacobian and diffusion matrices are*

$$J = \begin{pmatrix} -\theta & \theta - \mu \\ 0 & -(\gamma + p\mu) \end{pmatrix}, \quad \Sigma = \begin{pmatrix} \lambda + \mu s^* + \theta(q^* - s^*) & -\mu s^* \\ -\mu s^* & p\mu s^* + \gamma(c - s^*) \end{pmatrix},$$

which yields the following stationary second moments:

$$\begin{aligned} \text{Var}(Q) \approx v_{qq}^* &= \frac{\lambda}{\theta}, & \text{Var}(S) \approx v_{ss}^* &= \frac{c\gamma p\mu}{(\gamma + p\mu)^2}, \\ \text{Cov}[Q, S] \approx v_{qs}^* &= \frac{c\gamma p\mu}{(\gamma + p\mu)^2} \cdot \frac{\gamma + \theta + p\mu - \mu}{\theta + \gamma + p\mu}. \end{aligned}$$

*Proof.* The proof can be found in Appendix A.4.  $\square$

Notice that, in overload,  $\text{Cov}[Q, S]$  can be *negative*: a larger  $S$  boosts service capacity and pushes  $Q$  down. From the formula,

$$\text{sign}(\text{Cov}[Q, S]) = \text{sign}(\gamma + \theta + p\mu - \mu).$$

If service is fast and abandon/return are modest ( $\mu$  large relative to  $\gamma + \theta + p\mu$ ), then  $\text{Cov}[Q, S] < 0$ . Only when return/abandon feedback is sufficiently strong ( $\gamma + \theta$  large compared to the net service drain  $\mu(1 - p)$ ) can  $\text{Cov}[Q, S]$  turn positive, which is atypical in our parameter ranges. If we look closer at the condition for the covariance  $\text{Cov}[Q, S]$  to be negative

$$\text{Cov}[Q, S] < 0 \quad \text{if and only if} \quad \mu > \mu_{\text{neg}} := \frac{\gamma + \theta}{1 - p},$$

that is, when the service rate  $\mu$  is sufficiently large relative to the return rate  $\gamma$  and abandonment rate  $\theta$ . However, to remain in the overloaded regime,  $\mu$  must also satisfy

$$\mu < \mu_{\text{OL}} := \frac{\lambda\gamma}{\gamma c - \lambda p},$$

when  $\gamma c - \lambda p > 0$ . Thus, negative covariance in overload can only occur when

$$\mu_{\text{neg}} < \mu < \mu_{\text{OL}}.$$

If the first inequality does not hold, then the covariance will be positive and still be in OL. On the other hand, if  $\gamma c - \lambda p \leq 0$ , then the system is overloaded for all  $\mu > 0$ , so any  $\mu > \mu_{\text{neg}}$  yields negative covariance.

**Example 1:** Take

$$\lambda = 12, \quad \gamma = 1, \quad \theta = 0.2, \quad p = 0.3, \quad c = 10.$$

Then

$$\mu_{\text{neg}} = \frac{1 + 0.2}{1 - 0.3} \approx 1.714, \quad \mu_{\text{OL}} = \frac{12 \times 1}{10 - 12 \times 0.3} = \frac{12}{6.4} \approx 1.875.$$

For any  $\mu \in (1.714, 1.875)$ , the system is both overloaded and has negative covariance between  $Q$  and  $S$ .

**Example 2:** If we take  $p = 0$ , we would end up with

$$\mu_{\text{neg}} = \gamma + \theta, \quad \mu_{\text{OL}} = \frac{\lambda}{\gamma}.$$

So negative covariance in the overloaded case can trivially happen when  $\lambda > 2\gamma$ .

On the other hand, if we analyze the forward equation for the second moment of  $Q$ , we see that there is a relation between the  $Q$  and  $S$ , giving us the following relation

$$\theta v_{qq} + (\mu - \theta) \text{Cov}[Q, S] = \lambda,$$

so that, compared to the uncoupled approximation  $v_{qq} = \lambda/\theta$ , a negative  $v_{qs}$  reduces  $v_{qq}$  in overload.

## 5 Staffing for Delay Targets

A central performance measure in our system is the probability of delay

$$\mathbb{P}(Q \geq S), \quad (16)$$

the probability that an arrival must wait before service begins. In the classical Erlang-S model the server capacity is a fixed constant. This performance measure is valuable for making staffing decisions and making sure that service level agreements (SLA's) are met. However, in our setting, the number of available servers,  $S$ , fluctuates because servers without sufficient charge are forced to charge up. This section develops two staffing approximations: one assuming a deterministic approximation for  $S$  and one incorporating the stochastic fluctuations of  $S$ .

### 5.1 Deterministic Approximation for Number of Servers

Suppose  $Q$  is approximately normal,  $Q \sim N(q^*, q^*)$ , and replace the random available-server count by its fluid steady-state limit i.e.  $S = s^*$ . And let  $\Phi(x)$  and  $\varphi(x)$  be the cdf and pdf of a normal distribution. Then

$$\mathbb{P}(Q \geq s^*) = \bar{\Phi}\left(\frac{s^* - q^*}{\sqrt{q^*}}\right) = \epsilon. \quad (17)$$

**Theorem 5.1** (Deterministic-server staffing). *Let  $q^*$  and  $s^*$  denote the steady-state fluid limits of the queue length and available-server process, respectively. If the delay probability target is  $\epsilon \in (0, 1)$  and  $Q \sim N(q^*, q^*)$ ,  $S = s^*$ , then the staffing level that achieves*

$$\mathbb{P}(Q \geq S) = \epsilon. \quad (18)$$

satisfies

$$s^* = q^* + \sqrt{q^* \Phi^{-1}(\epsilon)}. \quad (19)$$

In the under-loaded regime the fluid relations  $q^* = \lambda/\mu$  and  $s^* = c - \lambda p/\gamma$  yield

$$c_\epsilon = \frac{\lambda p}{\gamma} + \frac{\lambda}{\mu} + \sqrt{\frac{\lambda}{\mu} \Phi^{-1}(\epsilon)}. \quad (20)$$

In the overloaded regime, where  $q^* = \frac{\lambda - \frac{\gamma \mu c}{\gamma + p\mu}}{\theta} + \frac{\gamma c}{\gamma + p\mu}$  and  $s^* = \frac{\gamma c}{\gamma + p\mu}$ , the same approximation yields

$$c_\epsilon = \frac{\gamma + p\mu}{2\gamma\mu^2} \left[ 2\lambda\mu - \theta(\mu - \theta) z_\epsilon^2 + \sqrt{\left(2\lambda\mu - \theta(\mu - \theta) z_\epsilon^2\right)^2 - 4\gamma\lambda\mu\theta z_\epsilon^2} \right]. \quad (21)$$

where  $z_\epsilon = \Phi^{-1}(\epsilon)$ .

*Proof.* The proof can be found in Appendix A.5.1.  $\square$

## 5.2 Normal approximation for Number of Servers

The deterministic adjustment of Section 4.1 treats the number of available servers as a fixed constant equal to its fluid mean  $s^*$ . While this provides intuition, it ignores the stochastic fluctuations of both  $Q$  and  $S$  that occur in steady state. In particular, the event  $\{Q \geq S\}$  depends not only on the means but also on the joint variability of these two quantities. To capture this, we adopt a *bivariate normal approximation*, modeling both  $Q$  and  $S$  as Gaussian random variables centered at their fluid steady-state values  $q^*, s^*$ . We approximate

$$Q \sim \mathcal{N}(q^*, v_{qq}), \quad S \sim \mathcal{N}(s^*, v_{ss}),$$

where the variance of  $Q$  and  $S$  are taken as general terms.

**Lemma 5.2** (Delay probability under a bivariate normal model with covariance). *Let  $(Q, S)$  be jointly normal with means  $q^*, s^*$ , variances  $\text{Var}[Q] = v_{qq} > 0$ ,  $\text{Var}[S] = v_{ss} > 0$ , and covariance  $\text{Cov}[Q, S] = v_{qs}$  (equivalently, correlation  $\rho = v_{qs}/\sqrt{v_{qq}v_{ss}} \in [-1, 1]$ ). Then*

$$\Pr(Q \geq S) = \bar{\Phi}\left(\frac{s^* - q^*}{\sqrt{v_{qq} + v_{ss} - 2v_{qs}}}\right) = \bar{\Phi}\left(\frac{s^* - q^*}{\sqrt{v_{qq} + v_{ss} - 2\rho\sqrt{v_{qq}v_{ss}}}}\right).$$

*Proof.* Proof can be found in Appendix A.5.2.  $\square$

**Theorem 5.3** (Bivariate-normal staffing with covariance). *Fix a target delay probability  $\epsilon \in (0, 1)$  and let  $z_\epsilon = \bar{\Phi}^{-1}(\epsilon)$ . Assume a joint-normal steady-state approximation for  $(Q, S)$  and use the regime-specific (diffusion) second-order closures.*

**(a) Underloaded regime.** *With  $q^* = \lambda/\mu$ ,  $s^* = c - \lambda p/\gamma$  and the diffusion approximation  $v_{qq} = \lambda/\mu$ ,  $v_{ss} = \lambda p/\gamma$ ,  $v_{qs} = 0$ , the staffing level  $c_\epsilon$  that achieves  $\Pr(Q \geq S) \approx \epsilon$  is*

$$c_\epsilon = \frac{\lambda p}{\gamma} + \frac{\lambda}{\mu} + z_\epsilon \sqrt{\frac{\lambda}{\mu} + \frac{\lambda p}{\gamma}}. \quad (22)$$

**(b) Overloaded regime.** *Let  $\kappa = \frac{\gamma}{\gamma + p\mu}$  so that  $s^* = \kappa c$  and  $q^* = \frac{\lambda}{\theta} + \kappa c \left(1 - \frac{\mu}{\theta}\right)$ . With diffusion (OU) second-order terms*

$$v_{qq} = \frac{\lambda}{\theta}, \quad v_{ss} = \frac{c \gamma p \mu}{(\gamma + p\mu)^2}, \quad v_{qs} = \frac{c \gamma p \mu}{(\gamma + p\mu)^2} \cdot \frac{\gamma + \theta + p\mu - \mu}{\theta + \gamma + p\mu},$$

*the staffing level  $c_\epsilon$  that achieves  $\Pr(Q \geq S) \approx \epsilon$  is*

$$c_\epsilon = \frac{2\mu\kappa\lambda + z_\epsilon^2\theta^2U + \sqrt{(2\mu\kappa\lambda + z_\epsilon^2\theta^2U)^2 - 4\mu^2\kappa^2(\lambda^2 - z_\epsilon^2\theta\lambda)}}{2\mu^2\kappa^2}, \quad (23)$$

*where*

$$U := \kappa\left(1 - \frac{\mu}{\theta}\right) - \frac{2\gamma p \mu}{(\gamma + p\mu)^2} \cdot \frac{\gamma + \theta + p\mu - \mu}{\theta + \gamma + p\mu}.$$

*Proof.* The proof can be found in Appendix A.5.3.  $\square$

## 6 Abandonment Targets

Another important performance measure for this queueing system is the expected excess number of customers in the system over the available servers, which directly relates to the expected number of abandonments. This section develops a normal approximation for the expected excess. We usually compute the fraction of abandonment via

In this section we derive performance guarantees and staffing rules for a target steady-state abandonment fraction

$$\alpha := \lim_{t \rightarrow \infty} \frac{N_{Ab}(t)}{N_A(t)} = \frac{\theta}{\lambda} \mathbb{E}[(Q - S)^+].$$

We develop a joint-normal approximation parallel to the delay analysis in Section 5, deriving closed-form expressions and implicit equations for the staffing level  $c$  required to achieve a specified abandonment target  $\alpha = \varepsilon$ .

### 6.1 Joint-normal expected excess

Let  $D := Q - S$ . Under the diffusion approximation from Section 4,

$$(Q, S) \stackrel{\text{d}}{\sim} \mathcal{N}\left((q^*, s^*), V\right), \quad V = \begin{pmatrix} v_{qq} & v_{qs} \\ v_{qs} & v_{ss} \end{pmatrix}.$$

Define

$$m := q^* - s^*, \quad \sigma^2 := v_{qq} + v_{ss} - 2v_{qs}.$$

**Lemma 6.1** (Expected positive part under bivariate normal). *If  $D \sim \mathcal{N}(m, \sigma^2)$  then*

$$\mathbb{E}[(Q - S)^+] = \mathbb{E}[D^+] = \sigma \varphi\left(\frac{m}{\sigma}\right) + m \Phi\left(\frac{m}{\sigma}\right).$$

*Proof.* You can find the proof in Appendix A.6. □

**Theorem 6.2** (Abandonment fraction under bivariate normal). *Under the joint-normal approximation,*

$$\alpha = \frac{\theta}{\lambda} \left[ \sigma \varphi\left(\frac{m}{\sigma}\right) + m \Phi\left(\frac{m}{\sigma}\right) \right], \quad m = q^* - s^*, \quad \sigma^2 = v_{qq} + v_{ss} - 2v_{qs}.$$

*Proof.* You can find the proof in Appendix A.6. □

Notice that this will give us a representation for the expected excess for a deterministic number of servers with a normal distribution of the queue length.

**Corollary 6.3** (Special cases). *If  $S \equiv s^*$  deterministically, then  $\sigma^2 = v_{qq}$  and*

$$\alpha = \frac{\theta}{\lambda} \left[ \sqrt{v_{qq}} \varphi\left(\frac{q^* - s^*}{\sqrt{v_{qq}}}\right) + (q^* - s^*) \Phi\left(\frac{q^* - s^*}{\sqrt{v_{qq}}}\right) \right].$$

*If  $Q$  and  $S$  are independent, then  $v_{qs} = 0$  so  $\sigma^2 = v_{qq} + v_{ss}$ .*

*Proof.* You can find the proof in Appendix A.6.  $\square$

## 6.2 Staffing for an abandonment target

We now solve for  $c$  such that  $\alpha = \varepsilon$ .

### 6.2.1 Underloaded regime ( $q^* < s^*$ )

In the UL regime the fluid system is never congested. Since

$$q^* = \frac{\lambda}{\mu}, \quad s^* = c - \frac{\lambda p}{\gamma}, \quad q^* < s^*,$$

all customers immediately enter service in the fluid limit, and the fluid queue, and hence the fluid abandonment fraction, is identically zero:

$$\alpha_{\text{fluid}} = \frac{\theta}{\lambda} (q^* - s^*)^+ = 0.$$

Diffusion fluctuations may cause rare excursions above  $s^*$ , producing occasional abandonments in steady state, but these events occur on an exponentially small scale in the staffing gap  $s^* - q^*$ . Thus, while the bivariate-normal approximation provides the expression

$$\alpha = \frac{\theta}{\lambda} \left[ \sigma \varphi(m/\sigma) + m \Phi(m/\sigma) \right], \quad m = q^* - s^* < 0,$$

the contribution is negligible whenever the system is meaningfully underloaded. Operationally, abandonment plays no role in determining staffing in UL: delay performance (Section 5) is the active constraint.

For this reason, abandonment-target staffing is relevant only in the over-loaded regime  $q^* > s^*$ , treated next.

### 6.2.2 Overloaded regime ( $q^* > s^*$ )

Recall  $s^* = \kappa c$  with  $\kappa = \gamma/(\gamma + p\mu)$  and

$$q^* = \frac{\lambda}{\theta} + s^* \left(1 - \frac{\mu}{\theta}\right), \quad m = \frac{\lambda}{\theta} - \frac{\mu\kappa}{\theta} c.$$

The second-order closures from Section 4 give

$$v_{qq} = \frac{\lambda}{\theta}, \quad v_{ss} = \frac{c\gamma p\mu}{(\gamma + p\mu)^2}, \quad v_{qs} = \frac{c\gamma p\mu}{(\gamma + p\mu)^2} \cdot \frac{\gamma + \theta + p\mu - \mu}{\theta + \gamma + p\mu},$$

and therefore

$$\sigma^2 = \frac{\lambda}{\theta} + U_A c, \quad U_A := \frac{\gamma p\mu}{(\gamma + p\mu)^2} \left(1 - 2 \frac{\gamma + \theta + p\mu - \mu}{\theta + \gamma + p\mu}\right).$$

**Theorem 6.4** (Abandonment-target staffing in OL). *For a target abandonment fraction  $\alpha = \varepsilon \in (0, 1)$ , the required staffing level  $c$  solves the monotone implicit equation*

$$\varepsilon = \frac{\theta}{\lambda} \left[ \sqrt{\frac{\lambda}{\theta} + U_A c} \varphi \left( \frac{\frac{\lambda}{\theta} - \frac{\mu\kappa}{\theta} c}{\sqrt{\frac{\lambda}{\theta} + U_A c}} \right) + \left( \frac{\lambda}{\theta} - \frac{\mu\kappa}{\theta} c \right) \Phi \left( \frac{\frac{\lambda}{\theta} - \frac{\mu\kappa}{\theta} c}{\sqrt{\frac{\lambda}{\theta} + U_A c}} \right) \right].$$

The right-hand side decreases strictly in  $c$ , so the solution is unique.

*Proof.* You can find the proof in Appendix A.6.  $\square$

This theorem characterizes  $c_\varepsilon$  as the unique root of a one dimensional nonlinear equation. In practice we solve this equation numerically. Let

$$\alpha(c) := \frac{\theta}{\lambda} \left[ \sigma(c) \varphi \left( \frac{m(c)}{\sigma(c)} \right) + m(c) \Phi \left( \frac{m(c)}{\sigma(c)} \right) \right], \quad (24)$$

then we can write the following proposition.

**Proposition 6.5** (Numerical staffing solution in OL). *Fix  $\varepsilon \in (0, \alpha_{\max})$  and let  $\alpha(c)$  be as in (24). Suppose we choose any bracket  $c_L < c_U$  in the OL region such that*

$$\alpha(c_L) > \varepsilon \geq \alpha(c_U).$$

*Then the unique solution  $c_\varepsilon$  of  $\alpha(c) = \varepsilon$  lies in  $[c_L, c_U]$  and can be found to arbitrary accuracy by any monotone root-finding scheme, such as bisection or Newton's method. In particular, the iterates stay within the bracket and converge to  $c_\varepsilon$ .*

*Proof.* You can find the proof in Appendix A.6.  $\square$

On the other hand, we can also include a feasibility condition, where we can lower bound the stochastic staffing requirement by a deterministic one. If we set up both the system size and the servers available as the steady state fluid limit, then we have the following:

**Proposition 6.6** (Fluid feasibility). *The fluid identity states in the over-loaded regime that  $s^* = \kappa c$  with  $\kappa = \gamma/(\gamma + p\mu)$  and*

$$q^* = \frac{\lambda}{\theta} + s^* \left(1 - \frac{\mu}{\theta}\right),$$

which yields

$$\alpha_{\text{fluid}} = 1 - \frac{\gamma\mu c}{\lambda(\gamma + p\mu)}.$$

Thus, any stochastic staffing solution must satisfy

$$c_\varepsilon \geq \frac{\lambda(\gamma + p\mu)}{\gamma\mu} (1 - \varepsilon).$$

*Proof.* You can find the proof in Appendix A.6.  $\square$

### 6.3 $(Q - S)^+$ and $(S - Q)^+$

In queueing systems with stochastic server availability, performance measures are often expressed in terms of excess demand or excess capacity. In particular, the random variables  $(Q - S)^+$  and  $(S - Q)^+$  represent, respectively, the instantaneous congestion beyond available capacity and the amount of idle service capacity. Moreover, we also know that the variance of  $(Q - S)^+$  is key in studying the tail risk of abandonment, which is directly controlled by CVar-type objectives. While earlier sections focus on mean performance measures, understanding the variability of these quantities is important for assessing the reliability of staffing rules and the dispersion of delay and abandonment outcomes. Under the bivariate-normal approximation for  $(Q, S)$ , both quantities reduce to the positive part of a Gaussian random variable, allowing their second-order properties to be characterized in closed form.

**Theorem 6.7** (Positive Part of a Normal Random Variable). *Let  $X \sim \mathcal{N}(\mu, \sigma^2)$  and define  $X^+ = \max\{X, 0\}$ . Let  $\alpha = \mu/\sigma$ , and denote by  $\phi(\cdot)$  and  $\Phi(\cdot)$  the standard normal pdf and cdf. Then*

$$\mathbb{E}[X^+] = \mu \Phi(\alpha) + \sigma \phi(\alpha),$$

$$\mathbb{E}[(X^+)^2] = (\mu^2 + \sigma^2)\Phi(\alpha) + \mu\sigma\phi(\alpha),$$

and

$$\text{Var}(X^+) = (\mu^2 + \sigma^2)\Phi(\alpha) + \mu\sigma\phi(\alpha) - (\mu\Phi(\alpha) + \sigma\phi(\alpha))^2.$$

*Proof.* You can find the proof in Appendix A.6.  $\square$

**Corollary 6.8.** *Let  $(Q, S)$  be jointly normal with  $Q - S \sim \mathcal{N}(m, \sigma^2)$ . Then*

$$\text{Var}[(Q - S)^+] = \text{Var}(X^+) \quad \text{with } X \sim \mathcal{N}(m, \sigma^2),$$

and

$$\text{Var}[(S - Q)^+] = \text{Var}(X^+) \quad \text{with } X \sim \mathcal{N}(-m, \sigma^2),$$

where  $\text{Var}(X^+)$  is given by the expression in Theorem 6.7.

Additional second-order properties and simulation results of excess demand under the joint-normal approximation are provided in Appendix B

## 7 Numerical Experiments

This section validates the fluid and diffusion approximations developed in Sections 3–4 by means of detailed event–driven simulations. Our goals are threefold: (i) to examine the accuracy of the fluid limits for  $(Q(t), S(t))$  across a wide range of parameters; (ii) to assess the quality of the second–order (diffusion) moments  $v_{qq}, v_{ss}, v_{qs}$ ; and (iii) to evaluate the operational staffing rules for delay and abandonment targets presented in Sections 5 and 6.

### 7.1 Simulation methodology

We implement an event–driven simulation that tracks the system state  $(Q(t), S(t))$  through arrival events, service completions, abandonment events, and transitions between active and charging server states. The simulator records a per–arrival snapshot of  $(Q, S)$ , time–averaged performance statistics, and cumulative abandonment and delay counts. Since the model is naturally event driven rather than time driven, we post process the event sequence into a regularly sampled time series to enable rolling moment estimates and trajectory plots.

To ensure robustness, we conduct a systematic parameter sweep covering over 5995 configurations (with 100,000 customers each); covering a broad

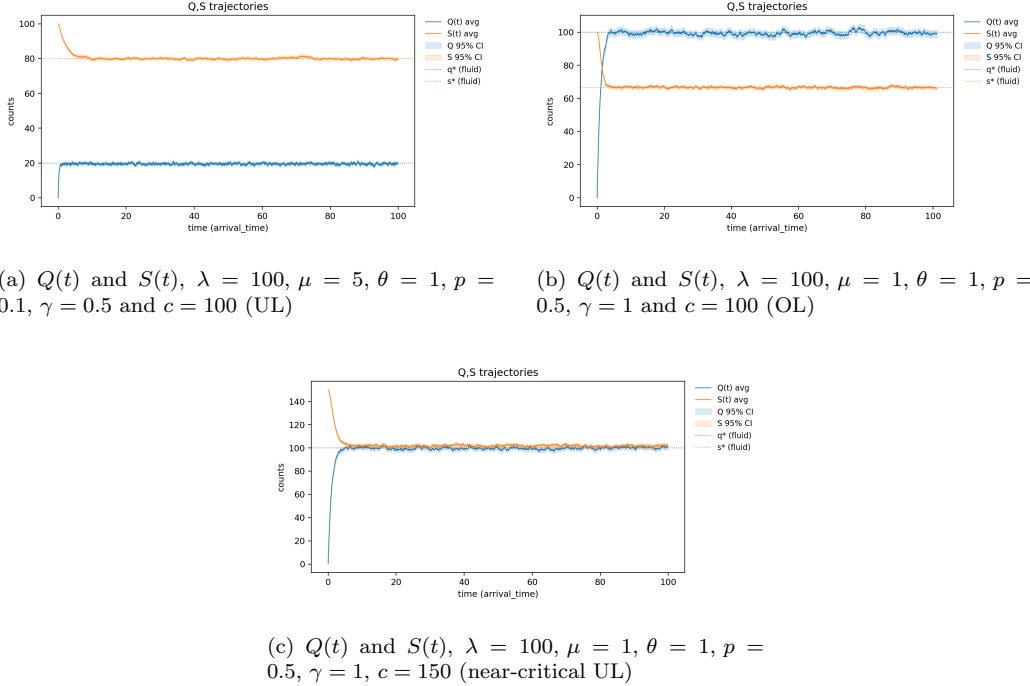


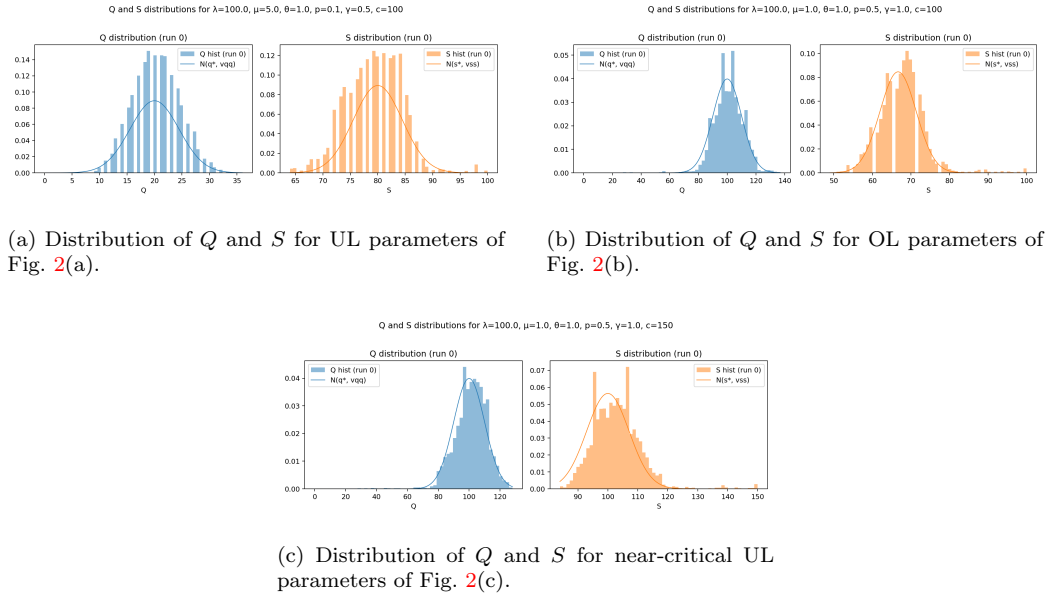
Figure 2:  $Q(t)$  and  $S(t)$  trajectories for 3 parameter sets and 100 simulation runs of 10,000 customers. Agreement with fluid limit is strong in all regimes.

range of arrival rates, service rates, abandonment rates, return rates, vacation (charging) probabilities, and staffing level that were selected from the following ranges:

$$\begin{aligned} \lambda &\in \{80, 100, 120\}, & \mu &\in \{0.5, 1, 10\}, & \theta &\in \{0.5, 1, 2\}, \\ p &\in \{0.1, 0.5, 0.8\}, & \gamma &\in \{0.1, 0.5, 1, 10\}, & c &\in [1, 1000]. \end{aligned}$$

The staffing levels used in this sweep were chosen so we could show the transition from UL to OL. For each configuration, we ran a single long simulation to estimate steady-state performance measures (delay probability, abandonment rate, average queue, etc.).

Because each run contained many customers, Monte Carlo noise for these coarse metrics is relatively small compared to the variation across parameter settings. We therefore use this sweep primarily to study qualitative trends and to compare fluid/diffusion approximations across a broad range of parameters, rather than to make precise point estimates with confidence



(a) Distribution of  $Q$  and  $S$  for UL parameters of Fig. 2(a). (b) Distribution of  $Q$  and  $S$  for OL parameters of Fig. 2(b).

(c) Distribution of  $Q$  and  $S$  for near-critical UL parameters of Fig. 2(c).

Figure 3: Empirical distributions of  $Q$  and  $S$  from a single simulation run compared with normal approximations based on fluid means and diffusion variances. Agreement is strong in OL and near-critical regimes; in heavily underloaded regimes, the empirical distributions are narrower due to constant server availability

intervals. For visualization, we focus on three representative configurations corresponding to UL, OL, and near-critical regimes.

For visualization and interpretation, we also include a collection of representative runs that illustrate the qualitative behavior of the dynamics in both UL and OL regimes. For these, we simulate 100 independent runs with 10,000 customers per run. We then average trajectories and moments across runs and construct pointwise confidence bands (which turn out to be very narrow).

In short, for the small number of representative parameter sets, we ran 100 independent replications and constructed confidence intervals using the classical-i.i.d. approach. For the large parameter sweep (5995 configurations) we used single long runs with time averaging to estimate steady-state quantities; these are primarily used to study trends and to compare fluid/diffusion approximations, rather than to report high-precision point estimates for each configuration.

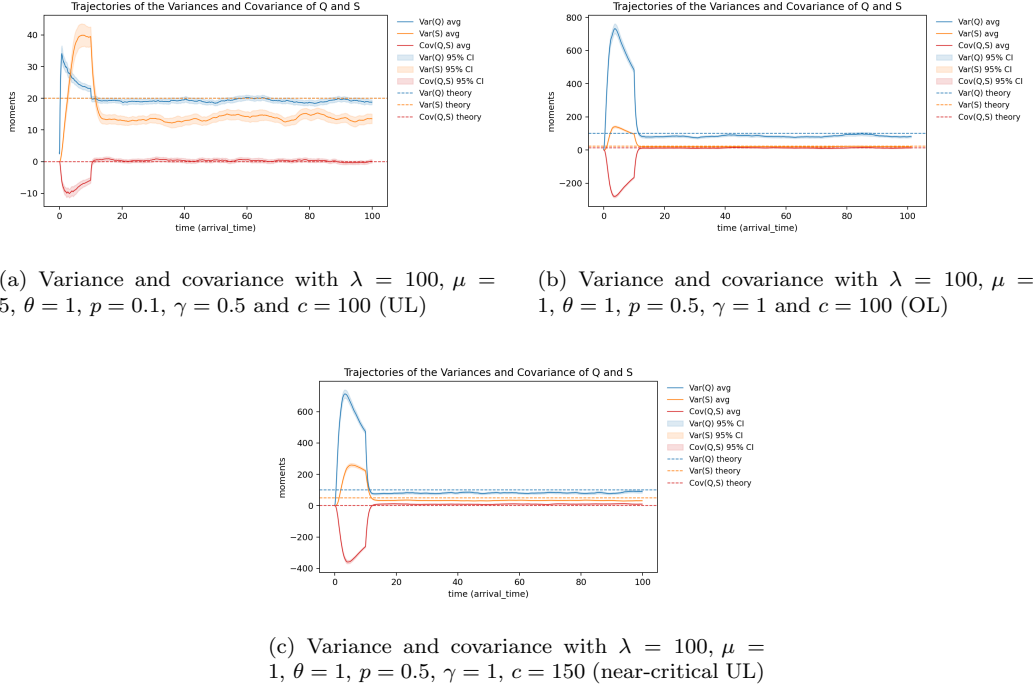


Figure 4:  $\text{Var}(Q(t))$ ,  $\text{Var}(S(t))$  and  $\text{Cov}(Q(t), S(t))$  trajectories for 3 parameter sets and 100 simulation runs of 10,000 customers. Agreement is strong in OL and near-critical regimes; in heavily underloaded regimes, the diffusion approximation overestimates server variance due to neglected stabilizing feedback.

## 7.2 Trajectory validation: fluid limits

Figure 2 shows sample paths of  $Q(t)$  and  $S(t)$  overlayed with their corresponding fluid fixed points. We show 3 plots for the different parameters. Each of them an average of 100 simulation runs. We can also see a small area around the plot lines, which are the confidence intervals. For the upper left plot we simulated an Under-loaded regime with  $\lambda = 100$ ,  $\mu = 5$ ,  $\theta = 1$ ,  $p = 0.1$ ,  $\gamma = 0.5$  and  $c = 100$ . Following Theorem 3.2, the steady state limits are  $q^* = 20$  and  $s^* = 80$ . In each regime, the trajectories fluctuate around the fluid predictions, with deviations consistent with the diffusion scale. For the upper right plot we simulated an Over-loaded regime, with  $\lambda = 100$ ,  $\mu = 1$ ,  $\theta = 1$ ,  $p = 0.5$ ,  $\gamma = 1$  and  $c = 100$ ,  $Q(t)$  stabilizes around 100 and  $S(t)$  concentrates near  $\kappa c = (1/1.5) \times 100 \approx 67$ , confirm-

ing the accuracy of Theorem 3.2. And for the bottom plot we simulated another Under-loaded regime, but on the boundary (i.e.  $\lambda/\mu + \lambda p/\gamma = c$ ) and we say is near-critical in the UL regime. The simulated parameters were  $\lambda = 100$ ,  $\mu = 1$ ,  $\theta = 1$ ,  $p = 0.5$ ,  $\gamma = 1$  and  $c = 150$ . And notice that, the same way as in the other UL run,  $Q(t)$  remains close to  $\lambda/\mu$  (for this run 100) while  $S(t)$  fluctuates around  $c - \lambda p/\gamma$  (for this run: 100).

On the other hand, Figure 3 compares the empirical distributions of  $Q$  and  $S$  from a single simulation run with their normal approximations  $\mathcal{N}(q^*, v_{qq})$  and  $\mathcal{N}(s^*, v_{ss})$ . For the three parameter sets, the histogram of  $Q$  and  $S$  for the overloaded and near-critical regimes are very close to the Gaussian curve, confirming accuracy of the diffusion approximation of the queue length.

In contrast, in a strongly under-loaded configuration with many idle servers ( $\lambda = 100$ ,  $\mu = 5$ ,  $\theta = 1$ ,  $p = 0.1$ ,  $\gamma = 0.5$ ,  $c = 100$ ), the empirical distribution of  $Q$  and  $S$  are noticeably tighter than  $\mathcal{N}(q^*, v_{qq} = \lambda/\mu)$  and  $\mathcal{N}(s^*, v_{ss} = \lambda p/\gamma)$ . This reflects a limitation of our UL diffusion closure: it effectively treats the system as an  $M/M/\infty$ -type queue with weak feedback, whereas in this regime the combination of fast service and abundant spare capacity induces very strong mean reversion. Upward fluctuations in the queue are eliminated quickly, and the interaction with the server-availability process further stabilizes the system, leading to underdispersion relative to the diffusion variance.

### 7.3 Diffusion validation: variances and covariance

To validate the diffusion closure, we compute rolling estimates of  $\text{Var}(Q(t))$ ,  $\text{Var}(S(t))$ , and  $\text{Cov}(Q(t), S(t))$  from the post-processed time series and compare them with the theoretical values  $v_{qq}, v_{ss}, v_{qs}$  obtained from the linear-Gaussian approximation.

Figure 4 displays the average of 100 simulation runs of empirical rolling moments together with the theoretical constants. The parameters used for the 3 runs are the same (and in the same order) as the ones used for computing the  $Q(t)$  and  $S(t)$  trajectories. This is,  $\lambda = 100$ ,  $\mu = 5$ ,  $\theta = 1$ ,  $p = 0.1$ ,  $\gamma = 0.5$  and  $c = 100$  for the upper-left;  $\lambda = 100$ ,  $\mu = 1$ ,  $\theta = 1$ ,  $p = 0.5$ ,  $\gamma = 1$  and  $c = 100$  for the upper-right; and  $\lambda = 100$ ,  $\mu = 1$ ,  $\theta = 1$ ,  $p = 0.5$ ,  $\gamma = 1$  and  $c = 150$  for the bottom. Note that we also give confidence regions around the average, which are negligible.

As expected,  $\text{Var}(S)$ ,  $\text{Var}(Q)$  and  $\text{Cov}[Q, S]$  match closely with its diffusion limit. There are slight variations in the simulation outputs in comparison

to the theory, but we can see the tendency of convergence of these results.

It is also important to note that in strongly under-loaded regimes shown in figure 4(a), with very fast service and many idle servers, the diffusion approximation tends to overestimate the variance of the active-server process  $S$ . This reflects the fact that our UL closure neglects some stabilizing feedback between the queue and the server-availability process. Nevertheless, the approximation for the queue-length variance and for  $\text{Cov}[Q, S]$  remains accurate, and the resulting staffing rules are still very close to simulation. This matches well with the empirical distribution shown in figure 3(a).

## 7.4 Operational validation: staffing for delay and abandonment

We next compare the staffing levels predicted by the fluid and diffusion rules with the minimum staffing empirically required to meet specified delay and abandonment targets.

$\lambda$	$\mu$	$\theta$	$p$	$\gamma$	$\varepsilon_{\text{delay}}$	$c_{\text{sim}}$	$c_{\text{fluid}}$	% (sim)	$c_{\text{diff}}$	% (sim)
80	1	1	0.1	0.5	0.01	123	115.19	93.65%	117.02	95.14%
80	1	1	0.5	0.1	0.05	564	494.71	87.71%	516.04	91.50%
80	10	1	0.5	0.5	0.10	112	91.62	81.80%	100.02	89.30%
100	1	1	0.1	0.5	0.01	149	141.46	94.94%	143.50	96.31%
100	1	1	0.5	0.1	0.05	697	616.45	88.44%	640.29	91.86%
100	10	1	0.5	0.5	0.10	137	114.05	83.25%	123.44	90.10%
120	1	1	0.1	0.5	0.01	176	167.50	95.17%	169.75	96.45%
120	1	1	0.5	0.1	0.05	819	738.02	90.11%	764.14	93.30%
120	10	1	0.5	0.5	0.10	164	136.44	83.20%	146.72	89.46%

Table 2: Comparison of simulated minimal staffing with fluid and diffusion predictions for delay targets.

For each target level  $\varepsilon$  and parameter configuration, we compute: (i) the minimal staffing  $c_{\varepsilon}^{\text{sim}}$  achieving the target in simulation; (ii) the staffing  $c_{\varepsilon}^{\text{fluid}}$  obtained from the fluid rules in Sections 5–6; and (iii) the diffusion-based staffing  $c_{\varepsilon}^{\text{diff}}$  defined implicitly by Theorem 5.3 and Theorem 6.4. Tables 2 and 3 summarize these comparisons.

$\lambda$	$\mu$	$\theta$	$p$	$\gamma$	$\varepsilon_{\text{aband}}$	$c_{\text{sim}}$	$c_{\text{fluid}}$	% (sim)	$c_{\text{diff}}$	% (sim)
80	1	1	0.5	10	0.01	94	-	-	92.73	98.65%
80	1	1	0.5	10	0.05	84	-	-	82.99	98.80%
80	1	1	0.5	10	0.10	77	75.6	98.18%	76.73	99.65%
100	0.5	1	0.5	0.5	0.01	328	-	-	320.04	97.57%
100	0.5	1	0.5	0.5	0.05	299	285	95.32%	291.47	97.48%
100	0.5	1	0.5	0.5	0.10	283	270	95.41%	271.80	96.04%
120	1	1	0.5	0.1	0.01	814	-	-	786.16	96.58%
120	1	1	0.5	0.1	0.05	764	-	-	706.55	92.48%
120	1	1	0.5	0.1	0.10	715	648	90.63%	655.14	91.63%

Table 3: Comparison of simulated minimal staffing with fluid and diffusion predictions for abandonment targets.

Across all delay targets tested, the diffusion rule consistently narrows the gap between the fluid prediction and the empirical minimum, often matching  $c_{\varepsilon}^{\text{sim}}$  exactly. For abandonment targets in OL, the implicit bivariate-normal rule produces staffing levels within one or two servers of the simulation-optimal value, while the fluid rule provides a necessary but not sufficient lower bound, as expected.

These results demonstrate that the diffusion approximation offers substantial accuracy gains over the fluid model in staffing problems, while remaining computationally trivial once the single scalar equation  $\alpha(c) = \varepsilon$  is solved.

## 7.5 Summary

Taken together, the trajectory plots, rolling-moment comparisons, and staffing experiments confirm the accuracy and operational usefulness of the fluid and diffusion framework developed in this paper. The fluid model captures the dominant deterministic structure of  $(Q, S)$ , while the diffusion corrections provide accurate second-order information and enable reliable stochastic staffing decisions for both delay and abandonment targets.

## 8 Conclusion and Extensions

The Erlang- $S^*$  model developed in this paper provides a tractable yet expressive framework for analyzing service systems in which servers intermittently become unavailable due to stochastic "vacations", motivated here by drone charging cycles. By integrating multi-server queueing dynamics with probabilistic charging decisions and exponential return times, we obtain a system that preserves analytical structure while capturing a defining operational feature of drone delivery. Across fluid, diffusion, and simulation analyses, several consistent insights emerge.

**Systematic capacity loss and its operational consequences.** The diffusion limit reveals that the joint behavior of  $(Q, S)$  is governed by an Ornstein-Uhlenbeck process with nontrivial covariance structure. In the underloaded regime, the two processes largely decouple, reflecting that queue length fluctuations are driven primarily by arrivals/service, while server fluctuations are driven by a balance between charging and return events. By contrast, in overload, the coupling becomes central: changes in the number of available servers induce immediate and opposing responses in queue length, typically resulting in a negative covariance. This interaction directly influences operational performance metrics, especially when calculating delay or abandonment probabilities. Incorporating these second-order effects substantially improves staffing approximations over fluid-based predictions.

**Accuracy and practical value of the diffusion-based staffing rules.** A key goal of this paper is enabling reliable staffing decision for delay and abandonment targets. Simulation experiments show that the joint-normal staffing rules, which incorporates both variances and covariance of  $(Q, S)$ , consistently produce staffing estimates within a reasonable margin of error of the true simulation optimum across a wide parameter range. In contrast, fluid-only rules, while intuitive and computationally simple, systematically under-predict required capacity in comparison to the diffusion estimates, demonstrating that the stochasticity introduced by charging meaningfully affects performance. The diffusion-based rules thus offer a computationally lightweight yet highly more accurate method suitable for real-time planning scenario analysis.

**Interpretation for drone delivery and similar systems.** In drone delivery contexts, these results underscore the importance of energy management strategies. The analysis quantifies how charging frequency  $p$  and return rate  $\gamma$  shape system congestion: increasing  $\gamma$  has a multiplicative effect on operational availability, while reducing  $p$  can prevent overload altogether. The formulas derived here offer immediate managerial insight; for instance, quantifying the performance gains from adopting battery swapping or partial charging policies.

**Future work.** This work opens several natural directions for future study. Heterogeneous fleets, where drones differ in service rates, charging times, or flight capabilities, would lead to multi-class extensions and richer dynamics. Incorporating state-dependent charging decisions would turn the model into controlled stochastic system, enabling the study of optimal energy management policies. Introducing spatial structure would allow service and charging rates to depend on geography, bridging this queueing model with drone routing and dispatch problems. Alternative performance regimes, such as loss systems with blocking, would extend the Erlang-S\* framework to high-reliability or capacity-limited environments. These extensions all retain analytical tractability while offering substantial practical relevance.

It would also be of interest to apply different risk measures for staffing as in Pender [36]. We have developed staffing policies for approximately stabilizing delay probabilities and abandonment probabilities, however, it would be of interest to approximately stabilize risk measures or other important performance measures that are relevant in various application areas.

Finally, there has been substantial recent interest in analyzing overlap and overlapping times in queueing networks Boxma [5], Palomo and Pender [31], Pender et al. [38], Newman and Pender [30], Boxma et al. [7], Boxma and Pender [6]. It would be of interest to extend this work to stochastic server settings in order to understand the impact of server stochasticity on overlap times in queues.

## References

- [1] Eitan Altman and Uri Yechiali. Analysis of customers' impatience in queues with server vacations. *Queueing systems*, 52(4):261–279, 2006.

- [2] Autel Robotics. Evo ii pro drones. <https://www.autelrobotics.com/productdetail/evo-ii-pro-drones>, 2025. Accessed: 2025-12-11.
- [3] David Azriel, Paul D Feigin, and Avishai Mandelbaum. Erlang-S: A data-based model of servers in queueing networks. *Management Science*, 65(10):4607–4635, 2019.
- [4] Justin J Boutilier and Timothy CY Chan. Drone network design for cardiac arrest response. *Manufacturing & Service Operations Management*, 24(5):2407–2424, 2022.
- [5] Onno Boxma. The number of overlapping customers. *Operations Research Letters*, 57:107203, 2024.
- [6] Onno Boxma and Jamol Pender. Overlap times in the  $G/G/1$  queue via Laplace transforms. *Queueing Systems*, 109(1):10, 2025.
- [7] Onno Boxma, Lucas van Kreveld, and Jamol Pender. The Overlapping Time Distribution in the  $M/G/\infty$  Queue. *Working Paper*, 2025.
- [8] Jay R Brown and Maxim A Bushuev. Last mile delivery with drones: A carbon emissions comparison. *International Journal of Sustainable Transportation*, 18(9):791–802, 2024.
- [9] Mingliu Chen and Ming Hu. Courier dispatch in on-demand delivery. *Management Science*, 70(6):3789–3807, 2024.
- [10] Youngmin Choi and Paul M Schonfeld. Optimization of multi-package drone deliveries considering battery capacity. In *Proceedings of the 96th annual meeting of the transportation research board, Washington, DC, USA*, pages 8–12, 2017.
- [11] Sudipta Chowdhury, Adindu Emelogu, Mohammad Marufuzzaman, Sarah G Nurre, and Linkan Bian. Drones for disaster response and relief operations: A continuous approximation model. *International Journal of Production Economics*, 188:167–184, 2017.
- [12] Taner Cokyasar, Wenquan Dong, Mingzhou Jin, and İsmail Ömer Verbas. Designing a drone delivery network with automated battery swapping machines. *Computers & Operations Research*, 129:105177, 2021.

- [13] Spiros Dimou, Antonis Economou, and Demetrios Fakinos. The single server vacation queueing model with geometric abandonments. *Journal of Statistical Planning and Inference*, 141(8):2863–2877, 2011.
- [14] DJI. Support for mavic air 2. <https://www.dji.com/support/product/mavic-air-2>, 2025. Accessed: 2025-12-11.
- [15] AN Dudin, SR Chakravarthy, SA Dudin, and OS Dudina. Queueing system with server breakdowns and individual customer abandonment. *Quality Technology & Quantitative Management*, 21(4):441–460, 2024.
- [16] Miguel A Figliozzi. Carbon emissions reductions in last mile and grocery deliveries utilizing air and ground autonomous vehicles. *Transportation Research Part D: Transport and Environment*, 85:102443, 2020.
- [17] Akash Ghosh, Bibhuti Bhusan Dash, Sudhansu Shekhar Patra, Trilok Nath Pandey, Binod Kumar Pattanayak, and Utpal Chandra De. Performance evaluation of drones in fanets using queueing model. In *2023 International Conference on Sustainable Communication Networks and Application (ICSCNA)*, pages 43–48. IEEE, 2023.
- [18] Anne Goodchild and Jordan Toy. Delivery by drone: An evaluation of unmanned aerial vehicle technology in reducing co2 emissions in the delivery service industry. *Transportation Research Part D: Transport and Environment*, 61:58–67, 2018.
- [19] Pasquale Grippa, Doris A Behrens, Friederike Wall, and Christian Bettstetter. Drone delivery systems: Job assignment and dimensioning. *Autonomous Robots*, 43(2):261–274, 2019.
- [20] Hailong Huang, Andrey V Savkin, and Chao Huang. Drone routing in a time-dependent network: Toward low-cost and large-range parcel delivery. *IEEE Transactions on Industrial Informatics*, 17(2):1526–1534, 2020.
- [21] Behzad Khamidehi, Majid Raeis, and Elvino S Sousa. Dynamic resource management for providing qos in drone delivery systems. In *2022 IEEE 25th International Conference on Intelligent Transportation Systems (ITSC)*, pages 3529–3536. IEEE, 2022.

- [22] Charles Knessl and Johan SH van Leeuwaarden. Transient analysis of the Erlang A model. *Mathematical methods of operations research*, 82(2):143–173, 2015.
- [23] Benjamin Legros and Oualid Jouini. Transient staffing at the beginning of work. *International Journal of Production Research*, 62(17):6427–6443, 2024.
- [24] Miguel A Lejeune and Wenbo Ma. Drone-delivery network for opioid overdose: Nonlinear integer queueing-optimization models and methods. *Operations Research*, 73(1):86–108, 2025.
- [25] Weiliang Liu and Xu Sun. Energy-aware and delay-sensitive management of a drone delivery system. *Manufacturing & Service Operations Management*, 24(3):1294–1310, 2022.
- [26] Yang Liu, Rui Tang, Zhuangbin Shi, Mingwei He, and Long Cheng. Shared mobility choices in metro connectivity: shared bikes versus shared e-bikes. *Transportation*, pages 1–27, 2025.
- [27] William A Massey and Jamol Pender. Gaussian skewness approximation for dynamic rate multi-server queues with abandonment. *Queueing Systems*, 75(2):243–277, 2013.
- [28] William A Massey and Jamol Pender. Dynamic rate Erlang-A queues. *Queueing Systems*, 89(1):127–164, 2018.
- [29] Alexey A Munishkin, Priyank Pradeep, Kenny Chour, and Krishna M Kalyanam. Traffic flow analysis for package delivery drones using a queueing model. In *2023 IEEE/AIAA 42nd Digital Avionics Systems Conference (DASC)*, pages 1–9. IEEE, 2023.
- [30] Laurel Newman and Jamol Pender. Contagious Queues: Analyzing the Spread of Infection in the  $M/G/\infty$  Queue. *Working Paper*, 2025.
- [31] Sergio Palomo and Jamol Pender. The maximum overlap time in the  $M/M/1$  queue. *Statistics & Probability Letters*, 219:110322, 2025.
- [32] Parrot. Anafi usa. <https://www.parrot.com/en/drones/anafi-usa>, 2025. Accessed: 2025-12-11.

- [33] Jamol Pender. Gram Charlier expansion for time varying multiserver queues with abandonment. *SIAM Journal on Applied Mathematics*, 74(4):1238–1265, 2014.
- [34] Jamol Pender. A Poisson–Charlier approximation for nonstationary queues. *Operations Research Letters*, 42(4):293–298, 2014.
- [35] Jamol Pender. The truncated normal distribution: Applications to queues with impatient customers. *Operations Research Letters*, 43(1):40–45, 2015.
- [36] Jamol Pender. Risk measures and their application to staffing nonstationary service systems. *European Journal of Operational Research*, 254(1):113–126, 2016.
- [37] Jamol Pender, Shuang Tao, and Anders Wikum. A stochastic model for electric scooter systems. *arXiv preprint arXiv:2004.10727*, 2020.
- [38] Jamol Pender, Young Myoung Ko, and Jin Xu. The number of overlapping customers in Erlang-A queues: an asymptotic approach. *Probability in the Engineering and Informational Sciences*, pages 1–26, 2025.
- [39] Roberto Pinto, Michela Zambetti, Alexandra Lagorio, and Fabiana Pirola. A network design model for a meal delivery service using drones. *International Journal of Logistics Research and Applications*, 23(4):354–374, 2020.
- [40] Benjamín Pla, Pau Bares, Andre Aronis, and Augusto Perin. Demand-adapting charging strategy for battery-swapping stations. *Batteries*, 11(7):251, 2025.
- [41] Shireen Seakhoa-King, Paul Balaji, Nicolas Trama Alvarez, and William J Knottenbelt. Revenue-driven scheduling in drone delivery networks with time-sensitive service level agreements. In *Proceedings of the 12th EAI international conference on performance evaluation methodologies and tools*, pages 183–186, 2019.
- [42] Seyed Mahdi Shavarani, Sam Mosallaeipour, Mahmoud Golabi, and Gökhan İzbırak. A congested capacitated multi-level fuzzy facility location problem: An efficient drone delivery system. *Computers & Operations Research*, 108:57–68, 2019.

- [43] Skydio. Skydio product support. <https://www.skydio.com/>, 2025. Accessed: 2025-12-11.
- [44] Bo Sun, Xiaoqi Tan, and Danny HK Tsang. Optimal charging operation of battery swapping and charging stations with qos guarantee. *IEEE Transactions on Smart Grid*, 9(5):4689–4701, 2017.
- [45] Shuang Tao. *Limit theorems in queueing networks with applications to shared mobility and healthcare*. Cornell University, 2020.
- [46] Shuang Tao and Jamol Pender. The impact of smartphone apps on bike sharing systems. *arXiv preprint arXiv:2004.10008*, 2020.
- [47] Shuang Tao and Jamol Pender. A stochastic analysis of bike-sharing systems. *Probability in the Engineering and Informational Sciences*, 35(4):781–838, 2021.
- [48] Johan SH Van Leeuwaarden and Charles Knessl. Spectral gap of the Erlang A model in the halfin-whitt regime. *Stochastic Systems*, 2(1):149–207, 2013.
- [49] Xiaolei Xie, Xu Dai, and Zhi Pei. Empowering the capillary of the urban daily commute: Battery deployment analysis for the locker-based e-bike battery swapping. *Transportation Science*, 58(1):176–197, 2024.
- [50] Mohamed Afiq Hidayat Zailani, Raja Zahratul Azma Raja Sabudin, Rahana Abdul Rahman, Ismail Mohd Saiboon, Aniza Ismail, and Zaleha Abdullah Mahdy. Drone for medical products transportation in maternal healthcare: A systematic review and framework for future research. *Medicine*, 99(36):e21967, 2020.

## A Proof Sketches and Technical Details

### A.1 Proof of theorem (3.1)

*Proof.* Recall that we have by the strong approximation for Poisson processes (FLLN)

$$\begin{aligned}\frac{N_A(\lambda nt)}{n} &= \lambda t + \varepsilon_A^n(t), \\ \frac{N_B(nx)}{n} &= x + \varepsilon_B^n(x), \\ \frac{N_{Ab}(nx)}{n} &= x + \varepsilon_{Ab}^n(x), \\ \frac{N_C(nx)}{n} &= x + \varepsilon_C^n(x), \\ \frac{N_B(nx)}{n} \frac{1}{N_B(nx)} \sum_{i=1}^{N_B(nx)} \xi_i &= \bar{\xi}x + \delta^n(x),\end{aligned}$$

where  $\varepsilon_A^n(t)$ ,  $\varepsilon_B^n(t)$ ,  $\varepsilon_{Ab}^n(t)$ ,  $\varepsilon_C^n(t)$  are martingales of order  $O_p(n^{-1/2})$  uniformly on compact intervals.

Subtract the candidate fluid limit and use the Lipschitz properties of  $\min(\cdot, \cdot)$  and  $(\cdot)^+$  to obtain

$$\begin{aligned}\|(\bar{Q}^n, \bar{S}^n) - (\bar{q}, \bar{s})\|(t) &\leq \|(\bar{Q}^n(0), \bar{S}^n(0)) - (q_0, s_0)\| + o_p(1) \\ &\quad + L \int_0^t \|(\bar{Q}^n, \bar{S}^n) - (\bar{q}, \bar{s})\|(s) ds\end{aligned}$$

for some constant  $L > 0$ . Recall that

$$\begin{aligned}\bar{q}(t) &= q_0 + \lambda t - \mu \int_0^t \min\{\bar{q}(s), \bar{s}(s)\} ds - \theta \int_0^t (\bar{q}(s) - \bar{s}(s))^+ ds, \\ \bar{s}(t) &= s_0 + \gamma \int_0^t (c - \bar{s}(s)) ds - \mu \bar{\xi} \int_0^t \min\{\bar{q}(s), \bar{s}(s)\} ds.\end{aligned}$$

(Note that with this property, we can already conclude by Kurtz 1978 paper that this process converges to the fluid limit)

In other words we can say that:

$$0 \leq -|\bar{Q}^n(t) - \bar{q}(t)| + |\bar{Q}^n(0) - \bar{q}(0)| + \left| \frac{N_A(\lambda nt)}{n} - \lambda t \right| \quad (25)$$

$$+ \left| \frac{N_B \left( \mu n \int_0^t \min(\bar{Q}^n(s), \bar{S}^n(s)) ds \right)}{n} - \mu \int_0^t \min(\bar{Q}^n(s), \bar{S}^n(s)) ds \right| \quad (26)$$

$$+ \left| \mu \int_0^t \min(\bar{Q}^n(s), \bar{S}^n(s)) ds - \mu \int_0^t \min(\bar{q}(s), \bar{s}(s)) ds \right| \quad (27)$$

$$+ \left| \frac{N_{Ab} \left( \theta n \int_0^t (\bar{Q}^n(s) - \bar{S}^n(s))^+ ds \right)}{n} - \theta \int_0^t (\bar{Q}^n(s) - \bar{S}^n(s))^+ ds \right| \quad (28)$$

$$+ \left| \theta \int_0^t (\bar{Q}^n(s) - \bar{S}^n(s))^+ ds - \theta \int_0^t (\bar{q}(s) - \bar{s}(s))^+ ds \right|, \quad (29)$$

with (25), (26), (28) corresponding to the assumptions and the convergence of scaled Poisson processes by strong approximation. On the other hand, we know that (27), (29) contain the functions  $\min(\cdot)$  and  $(\cdot)^+$  that are 1-Lipschitz. Therefore

$$\begin{aligned} \left| \mu \int_0^t \min(\bar{Q}^n(s), \bar{S}^n(s)) ds - \mu \int_0^t \min(\bar{q}(s), \bar{s}(s)) ds \right| &\leq \mu \int_0^t |\bar{Q}^n(s) - \bar{q}(s)| \\ &\quad + |\bar{S}^n(s) - \bar{s}(s)| ds \\ \left| \theta \int_0^t (\bar{Q}^n(s) - \bar{S}^n(s))^+ ds - \theta \int_0^t (\bar{q}(s) - \bar{s}(s))^+ ds \right| &\leq \theta \int_0^t |\bar{Q}^n(s) - \bar{q}(s)| \\ &\quad + |\bar{S}^n(s) - \bar{s}(s)| ds. \end{aligned}$$

Analogously, we have that

$$0 \leq -|\bar{S}^n(t) - \bar{s}(t)| + |\bar{S}^n(0) - \bar{s}(0)| \quad (30)$$

$$+ \left| \frac{N_C \left( \gamma n \int_0^t (c - \bar{S}^n(s)) ds \right)}{n} - \gamma \int_0^t (c - \bar{S}^n(s)) ds \right| \quad (31)$$

$$+ \left| \gamma \int_0^t (c - \bar{S}^n(s)) ds - \gamma \int_0^t (c - \bar{s}(s)) ds \right| \quad (32)$$

$$+ \left| \frac{1}{n} \sum_{i=1}^{N_B(\mu n \int_0^t \min(\bar{Q}^n(s), \bar{S}^n(s)) ds)} \xi_i - \mu \bar{\xi} \int_0^t \min(\bar{Q}^n(s), \bar{S}^n(s)) ds \right| \quad (33)$$

$$+ \left| \mu \bar{\xi} \int_0^t \min(\bar{Q}^n(s), \bar{S}^n(s)) ds - \mu \bar{\xi} \int_0^t \min(\bar{q}(s), \bar{s}(s)) ds \right|, \quad (34)$$

with (30), (31), (33) corresponding to the assumptions, the convergence of scaled Poisson processes by strong approximation and the convergence of the random sum term. Moreover, the same as before, we know that (32), (34) contain the functions  $\min(\cdot)$  and a linear difference that are 1-Lipschitz. Hence

$$\begin{aligned} \left| \gamma \int_0^t (c - \bar{S}^n(s)) ds - \gamma \int_0^t (c - \bar{s}(s)) ds \right| &\leq \gamma \int_0^t |\bar{S}^n(s) - \bar{s}(s)| ds \\ \left| \mu \bar{\xi} \int_0^t \min(\bar{Q}^n(s), \bar{S}^n(s)) ds - \mu \bar{\xi} \int_0^t \min(\bar{q}(s), \bar{s}(s)) ds \right| &\leq \mu \bar{\xi} \int_0^t |\bar{Q}^n(s) - \bar{q}(s)| \\ &\quad + |\bar{S}^n(s) - \bar{s}(s)| ds. \end{aligned}$$

Now, notice that both inequalities depend on this term, so if we sum them and then bound the sum, this should give us the result we want. Let

$$E_n(t) := |\bar{Q}^n(t) - \bar{q}(t)| + |\bar{S}^n(t) - \bar{s}(t)|,$$

and collect all Poisson remainders into

$$\begin{aligned} A_n(T) := \sup_{0 \leq u \leq T} \left( &\left| \frac{N_A(\lambda n u)}{n} - \lambda u \right| + \left| \frac{N_B(\cdot)}{n} - \cdot \right| + \left| \frac{N_{Ab}(\cdot)}{n} - \cdot \right| \right. \\ &\left. + \left| \frac{N_C(\cdot)}{n} - \cdot \right| + \left| \frac{1}{n} \sum_{i \leq N_B(\cdot)} \xi_i - \bar{\xi} \right| \right). \end{aligned}$$

Then, we know that there exists an  $L > 0$  (independent of  $n$ ) such that for all  $t \in [0, T]$ ,

$$E_n(t) \leq E_n(0) + A_n(T) + L \int_0^t E_n(s) ds.$$

Now, lets define  $F_n(t) := \sup_{0 \leq u \leq t} E_n(u)$ , then we can deduce that

$$F_n(t) \leq E_n(0) + A_n(T) + L \int_0^t F_n(s) ds.$$

With this we can apply Grönwall's inequality

$$F_n(t) \leq (E_n(0) + A_n(T))e^{Lt} \Rightarrow \sup_{0 \leq u \leq t} E_n(u) \leq (E_n(0) + A_n(T))e^{Lt}$$

The initial conditions converge by assumption and  $A_n(T)$  converges as we showed before, so the right-hand side vanishes in probability, proving the claim.  $\square$

A standard Kurtz FLLN argument for time-changed Poisson processes and random sums applied to (1)–(2) yields (5)–(6). Uniqueness follows from Lipschitz continuity of the drift.

## A.2 Diffusion Limit and Lyapunov Solution, proof of Theorem 4.1

We verify the conditions of a functional central limit theorem for density-dependent Markov jump processes and identify the limiting Ornstein–Uhlenbeck dynamics.

*Proof.* Fix  $T > 0$ . The proof follows from the diffusion approximation theorem for density-dependent Markov jump processes. We outline the verification of the required conditions.

*Step 1: Poisson time-change representation.* The joint process  $X^n(t) = (Q^n(t), S^n(t))^\top$  is a continuous-time Markov chain with finitely many transition types corresponding to the primitive events: arrivals, service completions (with and without entering charging), returns from charging, and abandonments. Hence there exist independent unit-rate Poisson processes  $\{N_k\}_{k=1}^K$ ,

jump vectors  $\{\ell_k\}_{k=1}^K \subset \mathbb{R}^2$ , and state-dependent intensities  $\{\lambda_k^n(\cdot)\}_{k=1}^K$  such that

$$X^n(t) = X^n(0) + \sum_{k=1}^K \ell_k N_k \left( \int_0^t \lambda_k^n(X^n(u)) du \right).$$

Dividing by  $n$  yields the fluid-scaled decomposition

$$\bar{X}^n(t) = \bar{X}^n(0) + \int_0^t b(\bar{X}^n(u)) du + M^n(t),$$

where  $b(\cdot)$  is the fluid drift and  $M^n$  is a martingale term.

*Step 2: Linearization on the active face.* Let  $x^* = (q^*, s^*)^\top$  be an equilibrium of the fluid limit in the operating regime under consideration. On the corresponding *active face* (i.e., away from the switching boundary), the drift  $b(\cdot)$  is continuously differentiable in a neighborhood of  $x^*$ . Therefore,

$$b(x^* + h) = b(x^*) + Jh + o(\|h\|) \quad \text{as } h \rightarrow 0,$$

where  $J = \nabla b(x^*)$  is the Jacobian on the active face and  $b(x^*) = 0$ .

*Step 3: Martingale FCLT and identification of  $\Sigma$ .* Define  $\hat{X}^n(t) = \sqrt{n}(\bar{X}^n(t) - x^*)$ . After centering and scaling, we obtain

$$\hat{X}^n(t) = \hat{X}^n(0) + \int_0^t J \hat{X}^n(u) du + \hat{M}^n(t) + o_p(1),$$

uniformly on  $[0, T]$ , where  $\hat{M}^n(t) = \sqrt{n} M^n(t)$ . By the martingale functional central limit theorem,  $\hat{M}^n \Rightarrow \Sigma^{1/2} W$  in  $D([0, T], \mathbb{R}^2)$ , where  $W$  is a standard two-dimensional Brownian motion and

$$\Sigma = \sum_{k=1}^K \ell_k \ell_k^\top \lambda_k(x^*)$$

is the covariance-rate matrix obtained from the primitive event rates at  $x^*$ .

*Step 4: Continuous mapping.* The limiting integral equation

$$\hat{X}(t) = \hat{X}(0) + \int_0^t J \hat{X}(u) du + \Sigma^{1/2} W(t)$$

admits a unique strong solution because the drift is linear and globally Lipschitz. By the continuous mapping theorem applied to the stochastic integral equation, it follows that  $\hat{X}^n \Rightarrow \hat{X}$  in  $D([0, T], \mathbb{R}^2)$ , where  $\hat{X}$  solves

$$d\hat{X}(t) = J \hat{X}(t) dt + \Sigma^{1/2} dW(t).$$

□

### A.3 Covariance and Variance Computations for Under-loaded Regime, proof of Theorem 4.2.

*Proof.* Here the active faces are  $\min(q, s) = q$  and  $(q - s)^+ = 0$ . The fluid fixed point is  $q^* = \lambda/\mu$  and  $s^* = c - \lambda p/\gamma$ . Linearizing the fluid drift on this face yields

$$J_{\text{UL}} = \begin{pmatrix} -\mu & 0 \\ -p\mu & -\gamma \end{pmatrix}.$$

Each primitive event contributes its increment vector and mean rate at the fixed point:

event	increment $\nu_e$	rate at $(q^*, s^*)$
arrival	$(1, 0)$	$\lambda$
unmarked completion	$(-1, 0)$	$(1 - p)\mu q^*$
marked completion	$(-1, -1)$	$p\mu q^*$
return-from-charge	$(0, 1)$	$\gamma(c - s^*)$

Hence the diffusion matrix is

$$\Sigma_{\text{UL}} = \lambda \begin{pmatrix} 1 & 0 \\ 0 & 0 \end{pmatrix} + (1 - p)\mu q^* \begin{pmatrix} 1 & 0 \\ 0 & 0 \end{pmatrix} + p\mu q^* \begin{pmatrix} 1 & 1 \\ 1 & 1 \end{pmatrix} + \gamma(c - s^*) \begin{pmatrix} 0 & 0 \\ 0 & 1 \end{pmatrix}.$$

Using the mean balance  $\gamma(c - s^*) = p\mu q^*$  and  $q^* = \lambda/\mu$  simplifies this to

$$\Sigma_{\text{UL}} = \begin{pmatrix} 2\lambda & p\mu q^* \\ p\mu q^* & 2p\mu q^* \end{pmatrix}.$$

The stationary covariance  $V_{\text{UL}} = \text{Cov}_\pi(\hat{X})$  solves the Lyapunov equation

$$J_{\text{UL}} V_{\text{UL}} + V_{\text{UL}} J_{\text{UL}}^\top + \Sigma_{\text{UL}} = 0,$$

whose unique solution is

$$V_{\text{UL}} = \begin{pmatrix} \lambda/\mu & 0 \\ 0 & \lambda p/\gamma \end{pmatrix}.$$

Therefore

$$\text{Var}[Q] \approx v_{qq}^* = \frac{\lambda}{\mu}, \quad \text{Var}[S] \approx v_{ss}^* = \frac{\lambda p}{\gamma}, \quad \text{Cov}[Q, S] \approx 0,$$

□

## A.4 Covariance and Variance Computations for Over-loaded Regime, proof of Theorem 4.3

*Proof.* Here the active faces are  $\min(q, s) = s$  and  $(q - s)^+ = q - s$ . The fluid fixed point satisfies  $s^* = \kappa c$ ,  $\kappa = \gamma/(\gamma + p\mu)$ , and  $q^* = \frac{\lambda}{\theta} + s^*(1 - \frac{\mu}{\theta})$ . Linearizing on this face gives

$$J_{OL} = \begin{pmatrix} -\theta & -(\mu - \theta) \\ 0 & -(\gamma + p\mu) \end{pmatrix}.$$

Event increments and rates at  $(q^*, s^*)$  are now

event	increment $\nu_e$	rate at $(q^*, s^*)$
arrival	$(1, 0)$	$\lambda$
unmarked completion	$(-1, 0)$	$(1 - p)\mu s^*$
marked completion	$(-1, -1)$	$p\mu s^*$
abandonment	$(-1, 0)$	$\theta(q^* - s^*)$
return-from-charge	$(0, 1)$	$\gamma(c - s^*) = p\mu s^*$

which yields

$$\begin{aligned} \Sigma_{OL} = & \lambda \begin{pmatrix} 1 & 0 \\ 0 & 0 \end{pmatrix} + (1 - p)\mu s^* \begin{pmatrix} 1 & 0 \\ 0 & 0 \end{pmatrix} + p\mu s^* \begin{pmatrix} 1 & 1 \\ 1 & 1 \end{pmatrix} \\ & + \theta(q^* - s^*) \begin{pmatrix} 1 & 0 \\ 0 & 0 \end{pmatrix} + \gamma(c - s^*) \begin{pmatrix} 0 & 0 \\ 0 & 1 \end{pmatrix}. \end{aligned}$$

Using the mean identities  $q^* - s^* = (\lambda - \mu s^*)/\theta$  and  $\gamma(c - s^*) = p\mu s^*$ , this simplifies to

$$\Sigma_{OL} = \begin{pmatrix} 2\lambda & p\mu s^* \\ p\mu s^* & 2p\mu s^* \end{pmatrix}.$$

The stationary covariance  $V_{OL}$  solves

$$J_{OL} V_{OL} + V_{OL} J_{OL}^\top + \Sigma_{OL} = 0,$$

with the unique solution

$$V_{OL} = \begin{pmatrix} \lambda/\theta & \frac{p\mu s^* - (\mu - \theta) v_{ss}^*}{\theta + \gamma + p\mu} \\ \frac{p\mu s^* - (\mu - \theta) v_{ss}^*}{\theta + \gamma + p\mu} & \frac{p\mu}{\gamma + p\mu} s^* \end{pmatrix},$$

with

$$v_{ss}^* = \frac{p\mu}{\gamma + p\mu} s^* = \frac{c\gamma p\mu}{(\gamma + p\mu)^2}.$$

Equivalently,

$$\text{Var}[Q] \approx \frac{\lambda}{\theta}, \quad \text{Var}[S] \approx \frac{c\gamma p\mu}{(\gamma + p\mu)^2} \text{Cov}[Q, S] \approx \frac{c\gamma p\mu}{(\gamma + p\mu)^2} \cdot \frac{\gamma + \theta + p\mu - \mu}{\theta + \gamma + p\mu}.$$

□

## A.5 Staffing Quadratics

The joint-normal delay condition (19) reduces to a quadratic in  $c$  in both regimes; we report the larger root for target  $\varepsilon$ .

### A.5.1 Deterministic Servers, proof of Theorem 5.1

*Proof.* In the underloaded case, we have

$$\bar{\Phi} \left( \frac{s^* - q^*}{\sqrt{q^*}} \right) = \epsilon \tag{35}$$

$$\frac{s^* - q^*}{\sqrt{q^*}} = \bar{\Phi}^{-1}(\epsilon) \tag{36}$$

$$s^* = q^* + \sqrt{q^*} \bar{\Phi}^{-1}(\epsilon) \tag{37}$$

$$c - \frac{\lambda p}{\gamma} = \frac{\lambda}{\mu} + \sqrt{\frac{\lambda}{\mu}} \bar{\Phi}^{-1}(\epsilon) \tag{38}$$

This implies that

$$c_\epsilon \approx \frac{\lambda p}{\gamma} + \frac{\lambda}{\mu} + \sqrt{\frac{\lambda}{\mu}} \bar{\Phi}^{-1}(\epsilon). \tag{39}$$

Note that this is quite different than the case where the servers are not stochastic. We see a shift in the number of servers needed of  $\frac{\lambda p}{\gamma}$ .

In the overloaded case, we have

$$s^* = q^* + \sqrt{q^*} \bar{\Phi}^{-1}(\epsilon) \quad (40)$$

$$\frac{\gamma}{\gamma + p\mu} c = \frac{\lambda - \frac{\gamma\mu c}{\gamma + p\mu}}{\theta} + \frac{\gamma c}{\gamma + p\mu} + \sqrt{\frac{\lambda - \frac{\gamma\mu c}{\gamma + p\mu}}{\theta} + \frac{\gamma c}{\gamma + p\mu}} \bar{\Phi}^{-1}(\epsilon) \quad (41)$$

$$\frac{\gamma\mu c}{\theta(\gamma + p\mu)} = \frac{\lambda}{\theta} + \sqrt{\frac{\lambda - \frac{\gamma\mu c}{\gamma + p\mu}}{\theta} + \frac{\gamma c}{\gamma + p\mu}} \bar{\Phi}^{-1}(\epsilon) \quad (42)$$

$$c = \frac{\lambda(\gamma + p\mu)}{\gamma\mu} + \frac{\theta(\gamma + p\mu)}{\gamma\mu} \sqrt{\frac{\lambda - \frac{\gamma\mu c}{\gamma + p\mu}}{\theta} + \frac{\gamma c}{\gamma + p\mu}} \bar{\Phi}^{-1}(\epsilon) \quad (43)$$

$$c = \frac{\lambda(\gamma + p\mu)}{\gamma\mu} + \frac{\theta(\gamma + p\mu)}{\gamma\mu} \sqrt{\frac{\lambda}{\theta} + \frac{\gamma c(\theta - \mu)}{\theta(\gamma + p\mu)}} \bar{\Phi}^{-1}(\epsilon) \quad (44)$$

Solving for  $c$ , simplifying, and writing down  $z_\epsilon = \bar{\Phi}^{-1}(\epsilon)$ , we get the desired expression

$$c_\epsilon = \frac{\gamma + p\mu}{2\gamma\mu^2} \left[ 2\lambda\mu - \theta(\mu - \theta) z_\epsilon^2 + \sqrt{\left(2\lambda\mu - \theta(\mu - \theta) z_\epsilon^2\right)^2 - 4\gamma\lambda\mu\theta z_\epsilon^2} \right].$$

□

### A.5.2 Delay Probability for Joint-Normal Distributed Queue and Server, proof of lemma 5.2

*Proof.* Define the difference  $D := Q - S$ . Since  $(Q, S)$  is jointly Gaussian and  $D$  is a fixed linear combination,  $D$  is Gaussian with

$$\begin{aligned} \mathbb{E}[D] &= q^* - s^* =: m, \\ \text{Var}[D] &= \text{Var}[Q] + \text{Var}[S] - 2\text{Cov}[Q, S] = v_{qq} + v_{ss} - 2v_{qs} =: \sigma^2. \end{aligned}$$

Thus  $D \sim \mathcal{N}(m, \sigma^2)$  and

$$\begin{aligned}
\Pr(Q \geq S) &= \Pr(D \geq 0) = \Pr\left(\frac{D - m}{\sigma} \geq \frac{-m}{\sigma}\right) \\
&= \Phi\left(\frac{m}{\sigma}\right) \\
&= \bar{\Phi}\left(\frac{-m}{\sigma}\right) \\
&= \bar{\Phi}\left(\frac{s^* - q^*}{\sqrt{v_{qq} + v_{ss} - 2v_{qs}}}\right).
\end{aligned}$$

The correlation form follows by substituting  $v_{qs} = \rho\sqrt{v_{qq}v_{ss}}$ .  $\square$

### A.5.3 Joint-normal Queue and Server Distribution for delay approximation, proof of Theorem 5.3

*Proof.* The joint-normal delay condition is

$$\begin{aligned}
\Pr(Q \geq S) &= \Phi\left(\frac{q^* - s^*}{\sqrt{\text{Var}[Q] + \text{Var}[S] - 2\text{Cov}[Q, S]}}\right) = \epsilon \\
\iff s^* &= q^* + z_\epsilon \sqrt{v_{qq} + v_{ss} - 2v_{qs}}. \tag{*}
\end{aligned}$$

(a) *Underloaded.* Insert  $q^* = \lambda/\mu$ ,  $s^* = c - \lambda p/\gamma$ , and the underloaded closures  $v_{qq} = \lambda/\mu$ ,  $v_{ss} = \lambda p/\gamma$ ,  $v_{qs} = 0$  into (\*):

$$c_\epsilon = \frac{\lambda p}{\gamma} + \frac{\lambda}{\mu} + z_\epsilon \sqrt{\frac{\lambda}{\mu} + \frac{\lambda p}{\gamma}} \tag{45}$$

which is the recommended staffing level.

(b) *Overloaded.* Write  $s^* = \kappa c$ ,  $q^* = \frac{\lambda}{\theta} + \kappa c(1 - \frac{\mu}{\theta})$ . Use the OU second-order terms listed in the theorem; then

$$v_{qq} + v_{ss} - 2v_{qs} = \frac{\lambda}{\theta} + U c, \quad U := \kappa\left(1 - \frac{\mu}{\theta}\right) - \frac{2\gamma p \mu}{(\gamma + p\mu)^2} \cdot \frac{\gamma + \theta + p\mu - \mu}{\theta + \gamma + p\mu}.$$

Plug into (\*) and isolate the square root:

$$\frac{\mu\kappa c - \lambda}{\theta} = z_\epsilon \sqrt{\frac{\lambda}{\theta} + U c}.$$

Square and rearrange to obtain the quadratic

$$\mu^2 \kappa^2 c^2 - (2\mu\kappa\lambda + z_\epsilon^2 \theta^2 U)c + (\lambda^2 - z_\epsilon^2 \theta\lambda) = 0,$$

whose larger root yields (23):

$$c_\epsilon = \frac{2\mu\kappa\lambda + z_\epsilon^2 \theta^2 U + \sqrt{(2\mu\kappa\lambda + z_\epsilon^2 \theta^2 U)^2 - 4\mu^2\kappa^2(\lambda^2 - z_\epsilon^2 \theta\lambda)}}{2\mu^2\kappa^2}$$

□

## A.6 Expected Abandonment proofs

### A.6.1 Proof of Lemma 6.1

Let  $D := Q - S \sim \mathcal{N}(m, \sigma^2)$ . The classical identity for a normal random variable states

$$\mathbb{E}[D^+] = \sigma \varphi\left(\frac{m}{\sigma}\right) + m \Phi\left(\frac{m}{\sigma}\right).$$

A direct proof is by integrating  $\int_0^\infty x f_D(x) dx$  and completing the square, or by noting  $D = m + \sigma Z$  with  $Z \sim \mathcal{N}(0, 1)$  and applying  $\mathbb{E}[(m + \sigma Z)^+]$ . Substituting  $D = Q - S$  yields the statement. □

### A.6.2 Proof of Theorem 6.2

By definition,

$$\alpha = \frac{\theta}{\lambda} \mathbb{E}[(Q - S)^+] = \frac{\theta}{\lambda} \mathbb{E}[D^+].$$

Applying Lemma 6.1 with  $D \sim \mathcal{N}(m, \sigma^2)$ ,  $m = q^* - s^*$  and  $\sigma^2 = v_{qq} + v_{ss} - 2v_{qs}$  gives

$$\alpha = \frac{\theta}{\lambda} \left[ \sigma \varphi\left(\frac{m}{\sigma}\right) + m \Phi\left(\frac{m}{\sigma}\right) \right].$$

□

### A.6.3 Proof of Corollary 6.3

If  $S \equiv s^*$  deterministically then  $\sigma^2 = v_{qq}$  and  $m = q^* - s^*$ ; substitute in Theorem 6.2. If  $Q$  and  $S$  are independent,  $v_{qs} = 0$  so  $\sigma^2 = v_{qq} + v_{ss}$ ; again substitute. □

#### A.6.4 Proof of Theorem 6.4

In OL,

$$s^* = \kappa c, \quad \kappa = \frac{\gamma}{\gamma + p\mu}, \quad q^* = \frac{\lambda}{\theta} + s^* \left(1 - \frac{\mu}{\theta}\right)$$

so

$$m(c) = q^* - s^* = \frac{\lambda}{\theta} - \frac{\mu\kappa}{\theta} c.$$

From the OU closures,

$$\sigma^2(c) = v_{qq} + v_{ss} - 2v_{qs} = \frac{\lambda}{\theta} + U_A c, \quad U_A = \frac{\gamma p \mu}{(\gamma + p\mu)^2} \left(1 - 2 \frac{\gamma + \theta + p\mu - \mu}{\theta + \gamma + p\mu}\right).$$

Define  $g(c) := \frac{\theta}{\lambda} [\sigma(c)\varphi(\frac{m(c)}{\sigma(c)}) + m(c)\Phi(\frac{m(c)}{\sigma(c)})]$ . Then  $\alpha = g(c)$  by Theorem 6.2. Note that  $m'(c) = -\mu\kappa/\theta < 0$  and  $\sigma'(c) = \frac{U_A}{2\sigma(c)}$  is  $O(c^{-1/2})$  for large  $c$ . Differentiating  $g$  gives us  $g'(c) < 0$ : the term driven by  $m'(c)$  dominates and the  $O(c^{-1/2})$  correction from  $\sigma'(c)$  cannot reverse monotonicity. Thus,  $g$  is strictly decreasing and the equation  $\alpha = \varepsilon$  has a unique solution in  $c$ . The displayed implicit equation is obtained by writing  $\alpha = g(c)$  explicitly.  $\square$

#### A.6.5 Proof of Proposition 6.5

*Proof.* By Theorem 6.4,  $\alpha(c)$  is continuous and strictly decreasing on the OL region, so the equation  $\alpha(c) = \varepsilon$  has a unique solution  $c_\varepsilon$  and the inequalities  $\alpha(c_L) > \varepsilon \geq \alpha(c_U)$  imply  $c_\varepsilon \in (c_L, c_U)$ . Bisection applied to the continuous, monotone function  $c \mapsto \alpha(c) - \varepsilon$  is guaranteed to converge to this root while maintaining the bracket. Newton's method, started from any point inside the bracket and combined with a standard line search or damping if needed, also converges to the unique root; see, e.g., standard numerical analysis texts. In both cases, the iterates remain in  $[c_L, c_U]$  and the error can be made arbitrarily small.  $\square$

#### A.6.6 Proof of Proposition 6.6

*Proof.* In OL, the fluid balance gives  $(q^* - s^*) = (\lambda - \mu s^*)/\theta$  with  $s^* = \kappa c$ . Hence

$$\alpha_{\text{fluid}} = \frac{\theta}{\lambda} (q^* - s^*)^+ = \left(1 - \frac{\mu s^*}{\lambda}\right)^+ = 1 - \frac{\gamma \mu c}{\lambda(\gamma + p\mu)}.$$

Thus any stochastic (joint-normal) design with  $\alpha = \varepsilon$  must satisfy  $c \geq \frac{\lambda(\gamma + p\mu)}{\gamma \mu} (1 - \varepsilon)$ .  $\square$

### A.6.7 Proof of Theorem 6.7

*Proof.* Let  $X \sim \mathcal{N}(\mu, \sigma^2)$  and define  $X^+ = \max\{X, 0\}$ . Write  $X = \mu + \sigma Z$  with  $Z \sim \mathcal{N}(0, 1)$ , and set  $\alpha = \mu/\sigma$ . Then

$$X^+ = (\mu + \sigma Z) \mathbf{1}\{\mu + \sigma Z > 0\} = (\mu + \sigma Z) \mathbf{1}\{Z > -\alpha\}.$$

Using linearity,

$$\mathbb{E}[X^+] = \mu \Pr(Z > -\alpha) + \sigma \mathbb{E}[Z \mathbf{1}\{Z > -\alpha\}].$$

Since  $\Pr(Z > -\alpha) = \Phi(\alpha)$ , it remains to compute  $\mathbb{E}[Z \mathbf{1}\{Z > a\}]$  for  $a = -\alpha$ . For  $Z \sim \mathcal{N}(0, 1)$  with density  $\phi$ , integration by parts gives

$$\mathbb{E}[Z \mathbf{1}\{Z > a\}] = \int_a^\infty z \phi(z) dz = \left[ -\phi(z) \right]_{z=a}^\infty = \phi(a),$$

because  $\phi(z) \rightarrow 0$  as  $z \rightarrow \infty$  and  $\phi'(z) = -z\phi(z)$ . With  $a = -\alpha$  and  $\phi(-\alpha) = \phi(\alpha)$ , we obtain

$$\mathbb{E}[X^+] = \mu \Phi(\alpha) + \sigma \phi(\alpha).$$

Similarly as how we computed the previous expectation, we have that,

$$\begin{aligned} \mathbb{E}[(X^+)^2] &= \mathbb{E}[(\mu + \sigma Z)^2 \mathbf{1}\{Z > -\alpha\}] \\ &= \mu^2 \Pr(Z > -\alpha) + 2\mu\sigma \mathbb{E}[Z \mathbf{1}\{Z > -\alpha\}] + \sigma^2 \mathbb{E}[Z^2 \mathbf{1}\{Z > -\alpha\}]. \end{aligned}$$

We already have  $\Pr(Z > -\alpha) = \Phi(\alpha)$  and  $\mathbb{E}[Z \mathbf{1}\{Z > -\alpha\}] = \phi(\alpha)$ . It remains to compute  $\mathbb{E}[Z^2 \mathbf{1}\{Z > a\}]$  with  $a = -\alpha$ :

$$\int_a^\infty z^2 \phi(z) dz = \int_a^\infty (\phi(z) - (z\phi(z))') dz = \int_a^\infty \phi(z) dz - \left[ z\phi(z) \right]_{z=a}^\infty = (1 - \Phi(a)) + a\phi(a).$$

(Here we used  $(z\phi(z))' = \phi(z) - z^2\phi(z)$  and again  $z\phi(z) \rightarrow 0$  as  $z \rightarrow \infty$ .) Substituting  $a = -\alpha$  yields

$$\mathbb{E}[Z^2 \mathbf{1}\{Z > -\alpha\}] = 1 - \Phi(-\alpha) + (-\alpha)\phi(-\alpha) = \Phi(\alpha) - \alpha\phi(\alpha).$$

Therefore

$$\begin{aligned} \mathbb{E}[(X^+)^2] &= \mu^2 \Phi(\alpha) + 2\mu\sigma \phi(\alpha) + \sigma^2 (\Phi(\alpha) - \alpha\phi(\alpha)) \\ &= (\mu^2 + \sigma^2)\Phi(\alpha) + \mu\sigma \phi(\alpha), \end{aligned}$$

since  $\alpha = \mu/\sigma$  implies  $\sigma^2\alpha\phi(\alpha) = \mu\sigma\phi(\alpha)$ .

Finally,

$$\text{Var}(X^+) = \mathbb{E}[(X^+)^2] - (\mathbb{E}[X^+])^2 = (\mu^2 + \sigma^2)\Phi(\alpha) + \mu\sigma \phi(\alpha) - (\mu\Phi(\alpha) + \sigma\phi(\alpha))^2.$$

This completes the proof.  $\square$

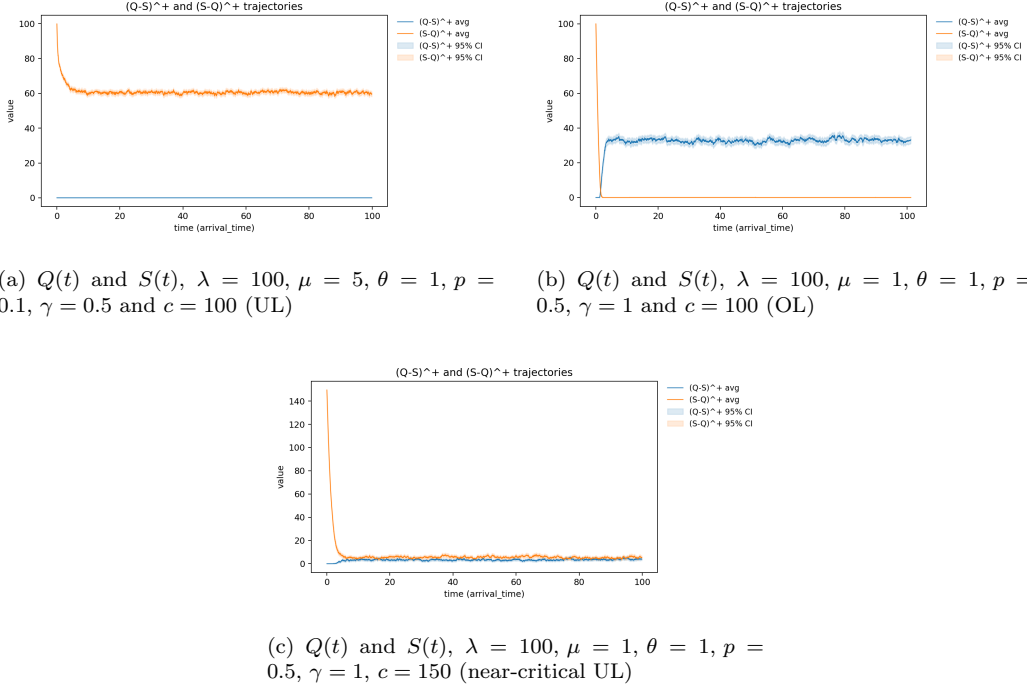


Figure 5:  $(Q(t) - S(t))^+$  and  $(S(t) - Q(t))^+$  trajectories for 3 parameter sets and 100 simulation runs of 10,000 customers.

## B Second-Order Properties of Excess Demand and Idle Capacity

The quantities  $(Q - S)^+$  and  $(S - Q)^+$  represent, respectively, excess demand beyond available service capacity and idle capacity in the system. While the main text focuses on mean performance measures such as delay probabilities and expected abandonment, the variability of these excess quantities plays a central role in risk-sensitive system design.

In particular, CVaR-based staffing formulations aim to control the tail behavior of congestion-related costs rather than their average value. For example, when congestion costs scale with  $(Q - S)^+$ , the conditional value-at-risk  $\text{CVaR}_\alpha((Q - S)^+)$  depends not only on the mean excess demand but also on its dispersion. Closed-form expressions for the variance of  $(Q - S)^+$  under the joint-normal approximation provide a tractable way to approximate tail risk and to compare staffing alternatives under worst-case or high-percentile

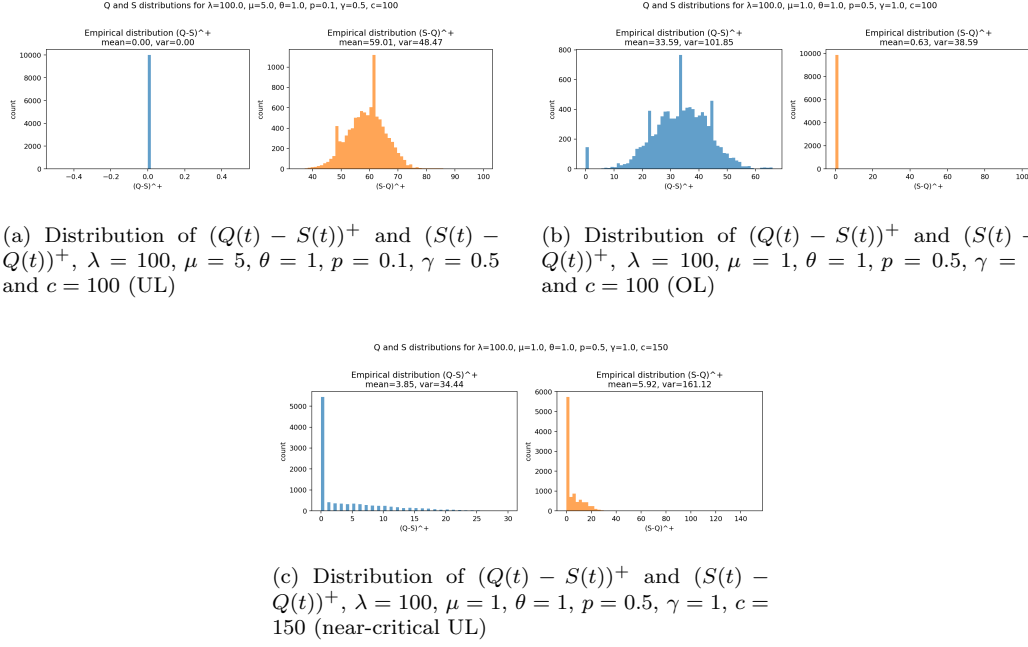


Figure 6: Empirical distributions of  $(Q(t) - S(t))^+$  and  $(S(t) - Q(t))^+$  from a single simulation run.

congestion scenarios.

Similarly, reliability guarantees often take the form of probabilistic constraints on extreme congestion events, such as ensuring that excess demand remains below a threshold with high probability. Variance information complements mean-based approximations by quantifying the spread of  $(Q - S)^+$  and enabling Gaussian or large-deviation approximations of reliability metrics. In systems with stochastic server availability, where congestion and capacity are endogenously coupled, these second-order effects are particularly important.

Finally, the variance of  $(S - Q)^+$  captures the dispersion of idle capacity, which is relevant in settings where over-staffing incurs explicit operational or energy costs. Risk-averse staffing policies may seek to balance the variability of congestion against the variability of idle resources, making joint consideration of both excess-demand and excess-capacity fluctuations essential. Although such risk-sensitive objectives are beyond the scope of this paper, the results in this appendix provide foundational tools for their analysis.

One of the results presented are the Figures 5 and 6. These experiments

reveal a sharp regime-dependent structure in the excess-demand and excess-capacity processes. In underloaded systems, congestion is essentially absent and variability concentrates entirely in idle capacity, while in overloaded systems the reverse holds. Near the critical boundary, both quantities exhibit heavy skewness and large variances driven by rare excursions, highlighting the limitations of mean-based performance metrics and motivating risk-sensitive staffing criteria.